cmgh
CELLULAR AND MOLECULAR GASTROENTEROLOGY AND HEPATOLOGY

ORIGINAL RESEARCH

Novel Fat Taste Receptor Agonists Curtail Progressive Weight Gain in Obese Male Mice

Amira Sayed Khan,[1] Aziz Hichami,[1] Babar Murtaza,[1] Marie-Laure Louillat-Habermeyer,[2] Christophe Ramseyer,[3] Maryam Azadi,[4] Semen Yesylevskyy,[3,5] Floriane Mangin,[2] Frederic Lirussi,[6] Julia Leemput,[1] Jean-Francois Merlin,[1] Antonin Schmitt,[6] Muhtadi Suliman,[1] Jérôme Bayardon,[2] Saeed Semnanian,[4] Sylvain Jugé,[2] and Naim Akhtar Khan[1]

[1]NUTox, UMR UB/AgroSup/INSERM U1231, Lipides, Nutrition & Cancer, LABEX-LipStick, Université de Bourgogne-Franche Comté (UBFC), Dijon, France; [2]ICMUB-OCS, UMR CNRS 6302, Université de Bourgogne-Franche Comté (UBFC), Dijon, France; [3]Laboratoire ChronoEnvironnement, UMR CNRS6249, Université de Bourgogne Franche-Comté (UBFC), Besançon, France; [4]Department of Physiology, Faculty of Medical Sciences, Tarbiat Modares University, Tehran, Iran; [5]Department of Physics of Biological Systems, Institute of Physics of the National Academy of Sciences of Ukraine, Kyiv, Ukraine; and [6]HSP-pathies, UMR UB/AgroSup/INSERM U1231, Lipides, Nutrition & Cancer, Université de Bourgogne-Franche Comté (UBFC), Dijon, France

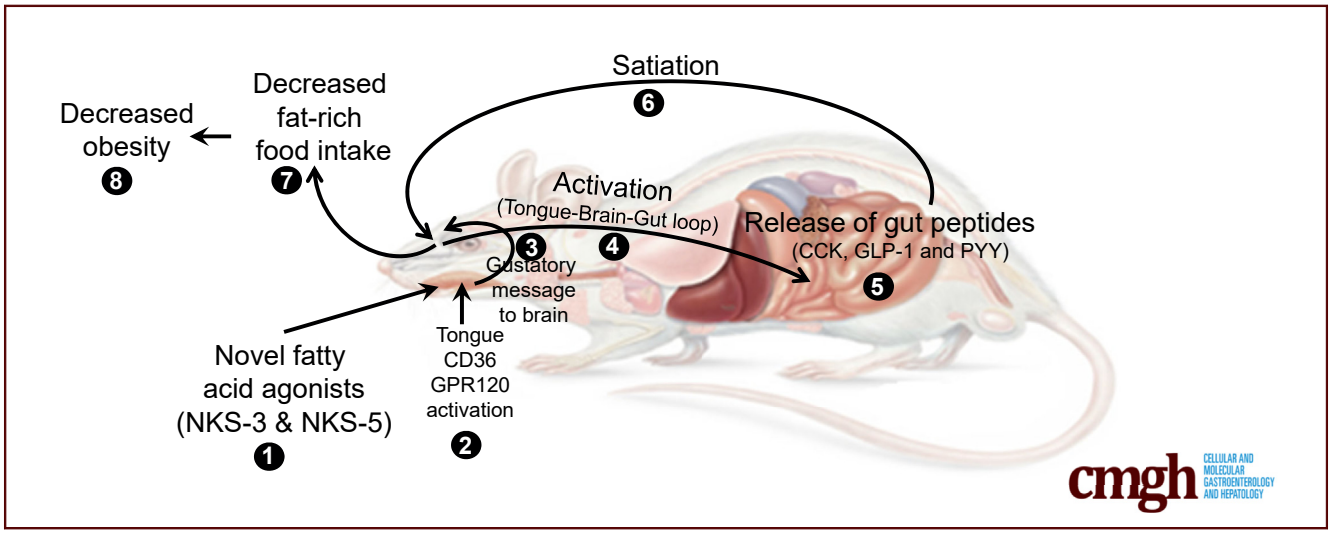

SUMMARY

Two high affinity agonists of tongue taste receptors (CD36/GPR120) were synthesized. They acted as fat taste enhancers and triggered the activation of tongue-gut satiation loop in male mice. These agents decreased daily fat-rich food intake and body weight gain in diet-induced obese male mice.

BACKGROUND & AIMS: The spontaneous preference for dietary lipids is principally regulated by 2 lingual fat taste receptors, CD36 and GPR120. Obese animals and most of human subjects exhibit low orosensory perception of dietary fat because of malfunctioning of these taste receptors. Our aim was to target the 2 fat taste receptors by newly synthesized high affinity fatty acid agonists to decrease fat-rich food intake and obesity.

METHODS: We synthesized 2 fat taste receptor agonists (FTA), NKS-3 (CD36 agonist) and NKS-5 (CD36 and GPR120 agonist). We determined their molecular dynamic interactions with fat taste receptors and the effect on Ca^{2+} signaling in mouse and human taste bud cells (TBC). In C57Bl/6 male mice, we assessed their gustatory perception and effects of their lingual application on activation of tongue-gut loop. We elucidated their effects on obesity and its related parameters in male mice fed a high-fat diet.

RESULTS: The two FTA, NKS-3 and NKS-5, triggered higher Ca^{2+} signaling than a dietary long-chain fatty acid in human and mouse TBC. Mice exhibited a gustatory attraction for these compounds. In conscious mice, the application of FTA onto the tongue papillae induced activation of tongue-gut loop, marked by the release of pancreato-bile juice into collecting duct and cholecystokinin and peptide YY into blood stream. Daily intake of NKS-3 or NKS-5 via feeding bottles decreased food intake and progressive weight gain in obese mice but not in control mice.

CONCLUSIONS: Our results show that targeting fat sensors in the tongue by novel chemical fat taste agonists might represent a new strategy to reduce obesity. *(Cell Mol Gastroenterol Hepatol 2023;15:633–663; https://doi.org/10.1016/j.jcmgh.2022.11.003)*

Keywords: Fat Taste; Lipids; CD36; GPR120; Obesity.

Recent evidences from rodent[1,2] and human[3] studies have demonstrated that besides 5 basic taste qualities, ie, sweet, sour, bitter, salt, and umami, there might be an additional sixth gustatory cue that is devoted to the perception of dietary fatty acids.[4,5] CD36, expressed by taste bud cells (TBC), has been shown to act as lipid sensor that is responsible for the gustatory detection of dietary long-chain fatty acids (LCFAs).[1,6–8] The CD36 deletion abolished preference for LCFAs and oily solutions in transgenic mice.[1] The gustatory lipid perception was also decreased significantly after small interfering RNA-targeted deletion of tongue CD36 in rats.[9] Also, G protein coupled receptor 40 (GPR40) and G protein coupled receptor 120 (GPR120) have been proposed to act as lipid sensors in the gustatory attraction of dietary lipids in mice, although GPR40 is absent in human beings.[4,10] The team of Sclafani[11] conducted studies on GPR120^{-}/$^{-}$ and CD36^{-}/$^{-}$ mice and demonstrated that the former is critical for post-oral but not oral, whereas the latter is involved in oral but not post-oral events of fat-rich food intake.[12] Our team also supported these conclusions and proposed that CD36 might be involved in immediate early detection, whereas GPR120 will be responsible for post-ingestive regulation of lipid food intake.[3–5] We have shown that LCFAs at low concentrations bind to CD36, whereas at high concentrations, these agents activate GPR120, and the 2 lipid sensors play non-overlapping but complementary roles in fatty acid–mediated signaling in human TBC.[3] It is also noteworthy that GPR120 and CD36 are co-expressed by the same TBC.[3] Hence, we can state that CD36 and GPR120 are principal candidate-regulators of fat eating behavior.

A number of experiments conducted on rodents (mice, rats, and gerbils) have suggested that obese animals exhibit low orosensory detection capacity for dietary fatty acids that, consequently, results in high fat intake.[4,5] In addition, a fat-rich diet that leads to obesity also alters fat taste perception. Multiple cross-sectional studies have confirmed these observations, viz, individuals who consume high levels of dietary fat exhibit reduced taste sensitivity to fatty acids.[13] Our laboratory has reported that Algerian,[14] Tunisian,[15,16] Moroccan,[17] and Czech[18] obese subjects exhibited an association with single nucleotide polymorphism of CD36, which is responsible for decreased CD36 protein expression and decreased orosensory perception of dietary fatty acids.

The cornerstone of therapeutic interventions to treat or prevent obesity is weight loss via lifestyle modifications, including hypocaloric dieting or detoxing and/or increased physical activity, but none of them is successful in the long run. In addition, the products such as inulin, maltodextrin, and plant fibers that mimic "fat-like" texture are not very successful because they do not trigger "fat-like taste", and their prolonged use may cause a number of gastrointestinal complications.[19] Because obese subjects exhibit dysfunctions of lingual fat taste receptors, which are responsible for low orogustatory perception of dietary lipids, it would be tempting to target lingual CD36 and GPR120 by non-caloric agents. Such kind of pharmacologic compounds would trigger fat-like taste, ideally more intense than natural dietary fatty acids, and trigger early satiation.

In the present study, we have synthesized 2 novel chemical compounds (see our recent patent [WO20192 29005 "Linoleic acid derivatives, pharmaceutical composition or food composition comprising said linoleic acid derivatives, and their uses", published on May 12, 2019]) on the basis of the structure of a dietary LCFA and assessed their effects on taste bud signaling, secretion of gut peptides, and intake of fat-rich food in diet-induced obese male mice. We demonstrate that tongue taste bud receptors such as CD36 and GPR120 can be the target of strategies to cut short dietary fat intake and, consequently, to combat obesity.

Results

Chemical Synthesis of Novel Fat Taste Receptor Agonists, Docking/Binding Calories With CD36 and GPR120 and Their Action on Taste Bud Calcium Signaling

The most common dietary LCFA that has been used as a taste receptor "ligand candidate" for in vitro and in vivo studies is linoleic acid (LA) because it is abundantly present in Western food because of increasing shift in food habits.[20] Hence, LA was used as the lead molecule to synthetize 2 fat taste receptor agonists (FTA), ie, NKS-3 (diethyl (9Z,12Z)-octadeca-9,12-dien-1-ylphosphonate; molecular weight, 386.56 daltons) and NKS-5 (9Z,12Z)-(3-methyloxetan-3-yl) methyl octadeca-9,12-dienoate; molecular weight, 364.57 daltons) (Figure 1*A*). The details on their chemical synthesis, involving a number of reactions and steps, can be seen in the Materials and Methods section.

At first hand, we were interested in the docking and kinetics of CD36 and GPR120 because no report is available on their behavior in the lipid bilayer. Hence, we used high-definition technology to assess this aspect in the artificial lipid bilayer of the plasma membrane. Figure 1*B* and *C* show

Abbreviations used in this paper: **AUC, area under the curve; [Ca^{2+}]i, intracellular calcium; CCK, cholecystokinin; CT, chorda tympani; CTA, conditioned taste aversion; FAS, fatty acid synthase; FTA, fat taste receptor agonists; GPCR, G protein-coupled receptor; GLP-1, glucagon-like peptide-1; GPR120, G protein coupled receptor 120; GPR40, G protein coupled receptor 40; HFD, high-fat diet; IL, interleukin; IPGTT, intraperitoneal glucose tolerance test; LA, linoleic acid; LCFA, long-chain fatty acid; LPS, lipopolysaccharide; OA, oleic acid; PB, pancreato-bile; PPAR-γ, peroxisome proliferator-activated receptor-γ; PYY, peptide YY; SCD1, stearoyl-CoA desaturase-1; SEM, standard error of the mean; SREBP1c, sterol-regulatory element-binding transcription factor 1c; SSO, sulfo-N-succinimidyl oleate; STD, standard diet; TBC, taste bud cells; TNF, tumor necrosis factor.**

Most current article

2352-345X
https://doi.org/10.1016/j.jcmgh.2022.11.003

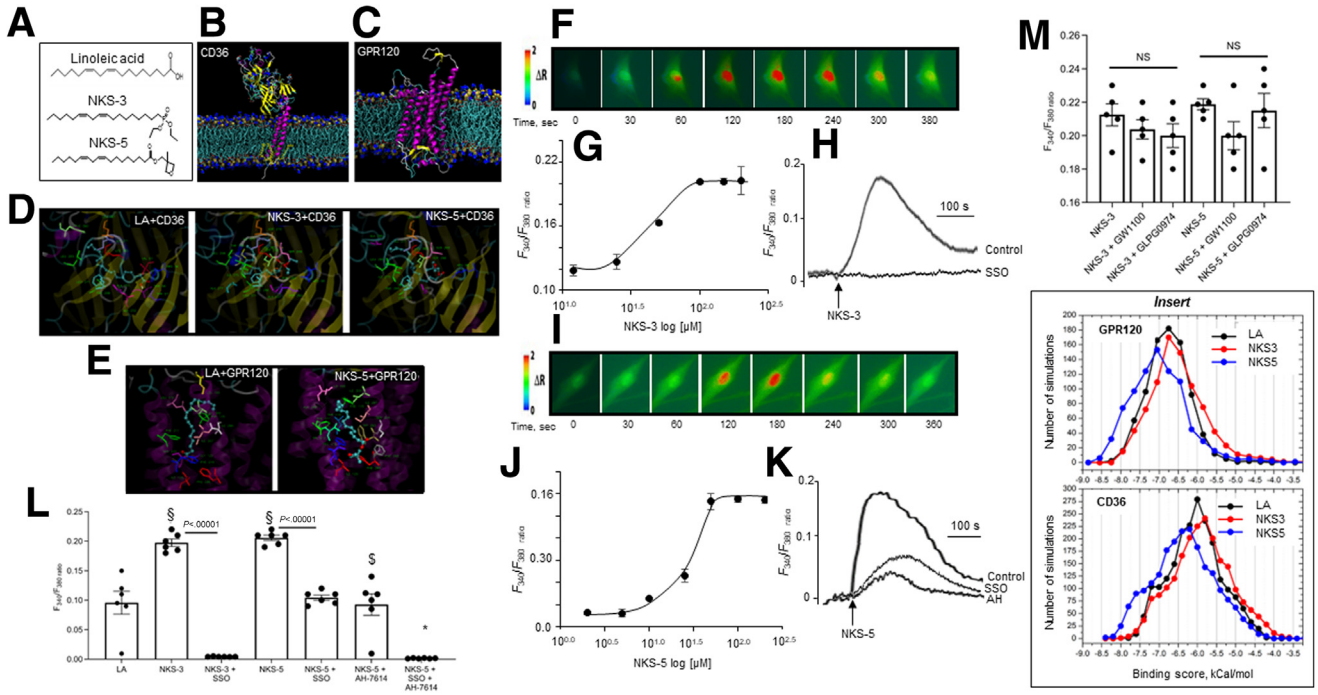

Figure 1. FTA bind to CD36/GPR120 and trigger Ca^{2+} signaling in TBC. (*A*) Structure of linoleic acid (LA), NKS-3 (diethyl (9Z,12Z)-octadeca-9,12-dien-1-ylphosphate; $C_{22}H_{43}PO_3$), and NKS-5 (9Z-12Z-methyloxetan-3-yl)methyl octadeca-9,12-dienoate; $C_{23}H_{40}O_3$). (*B* and *C*) Snapshots of equilibrated CD36 (*B*) and GPR120 (*C*) proteins in the plasma membrane environment. Proteins are shown as cartoon representation colored according to the secondary structure (helices are *purple*, beta-strands are *yellow*, turns are *cyan*, and unstructured loops are *white*). Lipids are shown as *sticks*, with N and P atoms of their head groups highlighted as *spheres*. For CD36 the glycosylated side chains are shown as *balls and sticks,* and the palmitoylated residues, visible in the lower monolayer, are colored *yellow*. Water and ions are not shown for clarity. (*D* and *E*) Docking/binding of LA, NKS-3, and NKS-5 with CD36 (*upper panel*) and GPR120 (*lower panel*) where the ligands are shown as *balls and sticks*, and protein is shown in semitransparent cartoon representation. The residues in contact with the ligands (within 0.3 nm from any ligand atom) are shown as *sticks* and are colored according to the residue index. For GPR120, the orientations of individual panels are not the same for clarity. *Insert* shows the distribution of the docking scores for GPR120 and CD36 proteins obtained for 834 protein conformations from molecular dynamic (MD) trajectories. Ca^{2+} signaling can be seen in human (*F–K*) and mouse (*L*) fungiform TBC (2×10^5 cells/assay), loaded with Fura-2/AM. The changes in $[Ca^{2+}]$i are expressed as F_{340}/F_{380} ratio. In *F* and *I*, the pseudo-colored time-lapse changes are seen as the increases in $[Ca^{2+}]_i$, evoked by NKS-3 and NKS-5, respectively, in human fungiform TBC. (*G* and *J*) Dose-dependent effects of NKS-3 and NKS-5, respectively. Each point shows the values as mean ± SEM (n = 6). *H* and *K*) Single traces of the action of NKS-3 and NKS-5, respectively, on the increases in $[Ca^{2+}]$i with and without preincubation for 15 minutes with CD36 inhibitor, ie, SSO (sulfo-*N*-succinimidyl oleate at 25 μmol/L), and GPR120 inhibitor, ie, AH (AH-7614 at 25 μM). (*L*) Ca^{2+} signaling by NKS-3 and NKS-5 with or without preincubation with SSO (25 μmol/L) or AH-7614 (25 μmol/L) for 15 minutes in mouse fungiform TBC (n = 6). NKS-3 and NKS-5 were used at 50 μmol/L (*F, H, L*) and 25 μmol/L (*I, K, L*), respectively. (*M*) Effect of antagonists of GPR40 (GW1100) and GPR43 (GLPG0974) on increases in $[Ca^{2+}]$i induced by NKS-3 and NKS-5 in Fura-2/AM loaded mouse fungiform TBC. Results show means ± SEM of n = 5 experiments with or without preincubation with GLPG0974 or GW1100 for 15 minutes. §Significant differences ($P < .003$) compared with LA-induced response at 20 μmol/L (*L*). *Statistically different data as compared with NKS-5-induced response ($P < .00006$). $^{\$}$Difference between NKS-5 vs NKS-5 plus AH (AH-7614) ($P < .0006$). Values are mean ± SEM. Unpaired two-tailed Student *t* test was used. NS, insignificant differences.

the snapshots of equilibrated lipid receptors in plasma membrane environment in the course of molecular dynamic simulations. Both proteins are stable and equilibrated well after 100 ns of simulations as monitored by their root-mean-square deviation from the starting structures. The extended flexible loops of GPR20 (residues 246-267 and 354-378) are moving in a chaotic manner during the simulations, but this does not affect the active site region of the protein and thus should not affect the docking simulations.

The best binding scores (in kcal/mol) for performed docking simulations for CD36 as regards LA, NKS-3, and NKS-5 are −8, −8, and −8.4, respectively. The best binding scores (in kcal/mol) for performed docking simulations for GPR120 as regards LA, NKS-3, and NKS-5 are −8.2, −8.1, and −8.6, respectively. These values are consistent with distributions (Figure 1 *insert*) and also suggest that the binding propensities of LA and NKS-3 are comparable, whereas NKS-5 binds significantly stronger than LA and NKS-3 with both the target proteins.

The contact probabilities differ only slightly between the ligands. However, it is clearly seen that for all residues, which form contacts with significant probability (more than

0.4), the values for NKS-3 and NKS-5 are systematically higher in comparison to LA. For NKS-5, binding probabilities are higher than for NKS-3, which is consistent with its better overall docking scores. This allows us to draw an important conclusion that both NKS-3 and NKS-5 bind to the same set of residues as LA but form stronger contacts with them.

The docking poses demonstrate that overall position of the ligands is mostly the same for LA, NKS-3, and NKS-5, but concrete residues in contact may differ (Figure 1*D* and *E*). NKS-5 exhibits higher binding energies than LA for both CD36 and GPR120, whereas the overall binding energy of NKS-3 and LA are comparable (Figure 1 *insert*). In our simulations, the following residues exhibited the highest probability to bind to the ligands: val^{61}, asn^{250}, leu^{251}, lys^{252}, phe^{266}, ala^{267}, ser^{268}, pro^{269}, val^{270}, glu^{271}, asn^{275}, asp^{295}, lys^{369}, leu^{371}, asn^{383}, thr^{385}, thr^{387}, and glu^{418} in CD36 and phe^{115}, thr^{119}, leu^{173}, leu^{196}, asp^{208}, phe^{211}, val^{212}, trp^{293}, ile^{296}, ile^{297}, and ile^{300} in GPR120.

As regards Ca^{2+} signaling, in human TBC, NKS-3 induced a rapid increase in intracellular free Ca^{2+} concentrations, $[Ca^{2+}]$i (Figure 1*F*–*H*) in a dose-dependent manner (Figure 1*G*). This agent exerted its action by binding to CD36 as a CD36 blocker (sulfo-*N*-succinimidyl oleate [SSO]) completely abolished its action in human (Figure 1*H*) and mouse (Figure 1*L*) TBC. NKS-5 induced an increase in $[Ca^{2+}]$i in human TBC (Figure 1*I*–*K*) via its action on both CD36 and GPR120 as SSO and AH-7614 (GPR120 antagonist) significantly curtailed increases in $[Ca^{2+}]$i in human (Figure 1*K*) and mouse (Figure 1*L*) TBC. Mice, but not human, TBC have been shown to express GPR40.[4,10] Interestingly, the 2 FTA did not induce an increase in $[Ca^{2+}]$i via GPR40 and also GPR43 because their respective inhibitors (GW1100 and GLPG0947) failed to decrease FTA-induced Ca^{2+} signaling in mouse TBC (Figure 1*M*).

FTA Activate Afferent Chorda Tympani Nerve and Tongue-Brain-Gut Loop

The fungiform papillae establish synaptic contacts with chorda tympani (CT) nerve, whereas circumvallate papillae are innervated by the glossopharyngeal nerve. To assess whether FTA gustatory message from fungiform TBC is sent to brain via CT nerve, we performed nerve recordings. The lingual application of NKS-3 and NKS-5 in conscious mice triggered rapid CT nerve responses that were higher than those triggered by dietary LCFAs such as LA and oleic acid (OA) (Figure 2). It is noteworthy that the addition of NKS-3 or NKS-5 to fatty acid–containing solutions further resulted in higher CT nerve recordings than those induced by fatty acids or FTA alone (Figure 2*B*–*E*).

To demonstrate the activation of tongue-brain-gut loop, we applied FTA onto the apical region of tongue epithelium, covering papillae regions, in conscious mice and quantified pancreato-bile (PB) secretion, having recuperated by a catheter (Figure 3 *insert*). NKS-5 induced higher PB secretion than LA and NKS-3 in the early phase (0–5 minutes and 10–15 minutes). Two FTAs induced higher PB secretion than LA at 3 time points, ie, 5–10 minutes, 15–20 minutes, and 25–30 minutes (Figure 3*A*). In the similar experimental set-up, we bled mice and observed that NKS-5 was more efficient than NKS-3 and LA on the release of cholecystokinin (CCK) at 30 and 60 minutes, although LA was better inducer than NKS-3 at these 2 time points (Figure 3*B*). As regards the release of peptide YY (PYY), NKS-5 was more potent than NKS-3 and LA at the same 2 time intervals (Figure 3*B* and *C*).

Mice Exhibit Spontaneous Preference for FTA That Modulate Gustatory Perception of Dietary Lipids

In the 2-bottle paradigm (Figure 4 *insert*), mice exhibited significant preference for NKS-3 at 50 μmol/L (Figure 4*A*) and NKS-5 at 75 μmol/L (Figure 4*B*), although at high concentrations, the 2 FTA failed to demonstrate the gustatory attraction in mice (Figure 4*A* and *B*). Figure 4*C*–*F* show that mice exhibit a strong preference for LA and canola oil, and the addition of NKS-3 and NKS-5 decreased their preference significantly. To avoid the post-ingestive mechanisms, we conducted short-term (1 and 5 minutes) licking experiments, and we noticed that FTA triggered higher licks than LA, and the mixture (LA plus FTA) still resulted in higher licks than LA alone (Figure 4*G* and *H*).

FTA Decrease Weight Gain in Obesity, Up-regulate Obesity-Induced Decreased Ca^{2+} Signaling to LCFA in TBC, and Modulate Gut Microbiota in Obese Male Mice

We maintained 8-week-old C57BL/6 male mice on a standard diet (STD) or a high-fat diet (HFD) for 10 weeks (for diet composition see Table 1). After 10 weeks of STD or HFD feeding, the animals were further divided into following groups: control group (HFD or STD), STD or HFD + NKS-3 (50 μmol/L), or NKS-5 (75 μmol/L). The mice received FTA in water bottles ad libitum for another 16 weeks (Figure 5*A*). Two FTA decreased the degree of obesity and food intake, where NKS-5 exerted more pronounced effect than NKS-3 on both the parameters (Figure 5*A* and *B*). The FTA failed to influence body weight and food intake in STD-fed animals (Figure 5*A* and *C*). HFD feeding increased fat mass, and the FTA decreased the same without influencing lean mass in obese animals (Figure 5*D*).

The expression of CD36 and GPR120 mRNA in mice TBC was decreased or increased, respectively, by HFD (Figure 5*E*). The Western blots demonstrate reduced and high protein expression of CD36 and GPR120, respectively, in TBC from HFD animals, and intake of FTA (NKS-3 and NKS-5) reversed this trend (Figure 5*F* and *G*). The reduced TBC Ca^{2+} signaling in obese animals is the striking feature of decreased taste perception of dietary fatty acids.[3] Interestingly, LA-induced decreases in $[Ca^{2+}]$i in TBC from obese mice were reversed when obese mice were given NKS-3 or NKS-5 (Figure 5*H*).

As regards daily energy expenditure, NKS-3, but not NKS-5, significantly increased energy expenditure in HFD-fed mice (Figure 6*A* and *B*, Table 2). In addition, consumption of NKS-3 by HFD mice increased locomotor activity (Figure 6*C*).

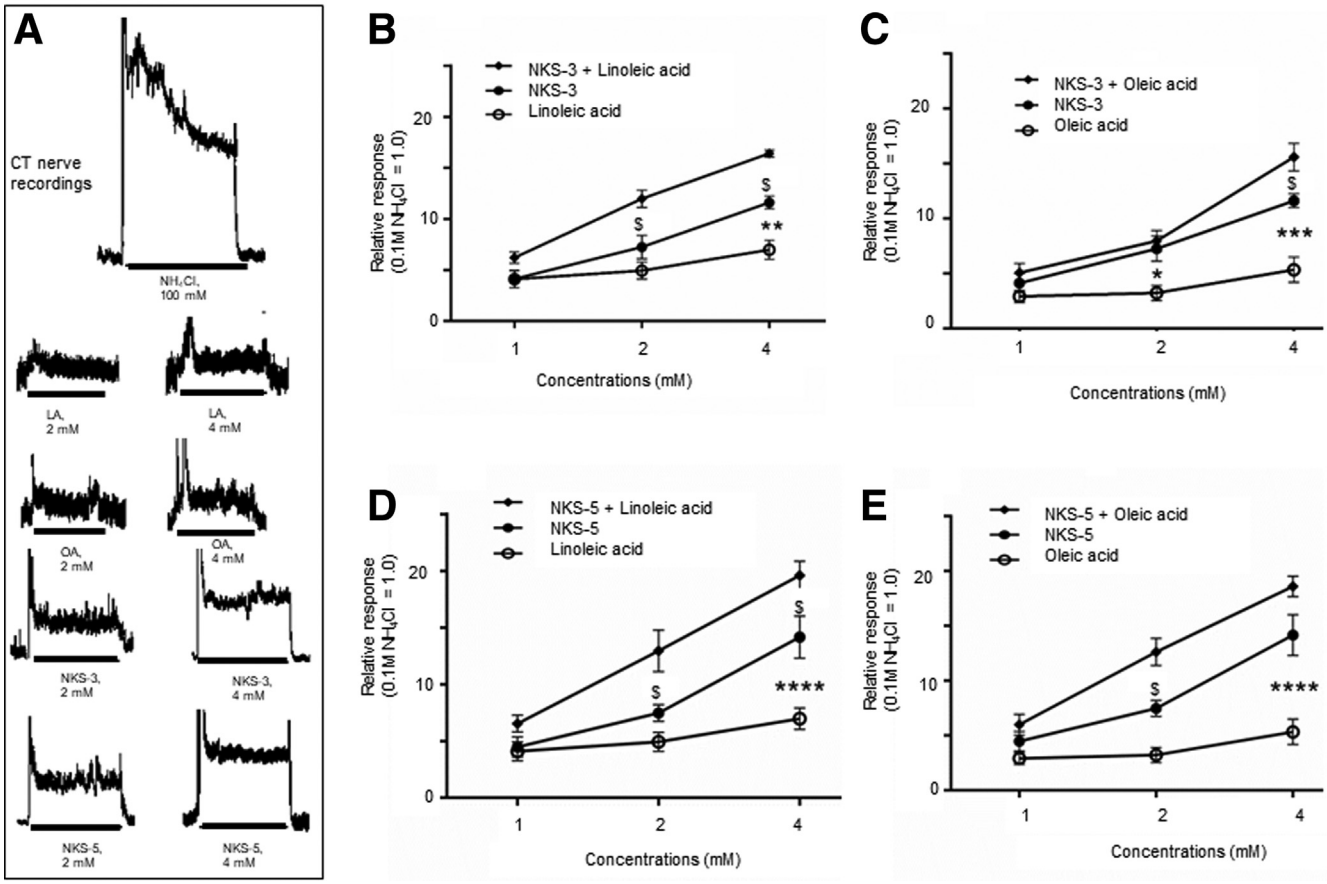

Figure 2. FTA activate afferent chorda tympani (CT) nerve in mice. (*A*) Single traces of whole nerve CT recordings, evoked by NH_4Cl, LA (linoleic acid), OA (oleic acid), NKS-3, and NKS-5 applications on tongue epithelium. (*B* and *E*) Dose-response relationship of integrated whole nerve CT responses. CT responses were normalized to NH_4Cl at 100 mmol/L. FTA and fatty acids were tested at different concentrations. (NKS-3 (*B*, *C*), n =6; NKS-5 (*D*, *E*), n = 7; linoleic acid (*B*, *D*), n = 11; oleic acid (*C*, *E*), n =4; NKS-3 + linoleic acid (*B*), n = 4; NKS-3 + oleic acid (*C*), n = 4; NKS-5 + linoleic acid (*D*), n = 4; NKS-5 + oleic acid (*E*), n = 4). Statistical significance between the groups was analyzed by means of repeated measure two-way analysis of variance, followed by Tukey multiple comparison test. Asterisks indicate differences between FTA and fatty acids groups, whereas $ indicates differences between FTA plus fatty acids vs FTA groups ($P < .05$). $^{**}P < .01$, $^{***}P < .001$, $^{****}P < .0001$.

Gut microbiota of the obese has been shown to be determinant in obesity.[21] The family level analysis of fecal microbiota of obese mice shows that these animals had high bacteria of Lachnospiraceae family that belongs to Firmicutes division (Figure 7*A*). We observed that STD-fed animals had high *Prevotella* species of bacteria of Bacteroidetes phylum (Figure 7*A*). NKS-3 and NKS-5 given to HFD-fed mice increased the bacteria of Marinifilaceae and Bacteroidaceae, respectively, families that belong to Bacteroidetes phylum. The linear discriminant analysis effect size is an algorithm for high-dimensional biomarker discovery and explanation that can identify taxonomic groups characterizing the differences between 2 or more biological conditions. It emphasizes both statistical significance and biological relevance to identify differentially abundant features that are also consistent with biologically meaningful categories (subclasses). The linear discriminant analysis effect size robustly identifies features that are statistically different among biological classes. The fecal linear discriminant analysis effect size observations in control diet fed animals, in accordance with several scientific reports,[22,23] exhibit high number of bacterial populations that belong to Verrucomicrobia phylum to whom also belongs *Akkermensia* (Figure 7*B*). Addition of NKS-3 to obese mice shifted the fecal bacterial population to another species (Figure 7*D*); most of them were unidentified. When obese animals were given NKS-5 in the water bottles, the fecal microbiota profile was marked by Verrucomicrobia phylum, and it was also different from obese mice that received NKS-3 (Figure 7*C* and *D*). These observations demonstrate that the 2 agents (NKS-3 and NKS-5) are "shifting" the gut microbial population to a different population that might be involved in the beneficial effects of these agents.

FTA Trigger the Release of Gut Peptides, Induce Insulin Sensitivity, Decrease Inflammation, and Normalize Dyslipidemia in Obese Mice

Intake of NKS-3 and NKS-5 in obese mice induced the release of glucagon-like peptide-1 (GLP-1), CCK-1, and PYY

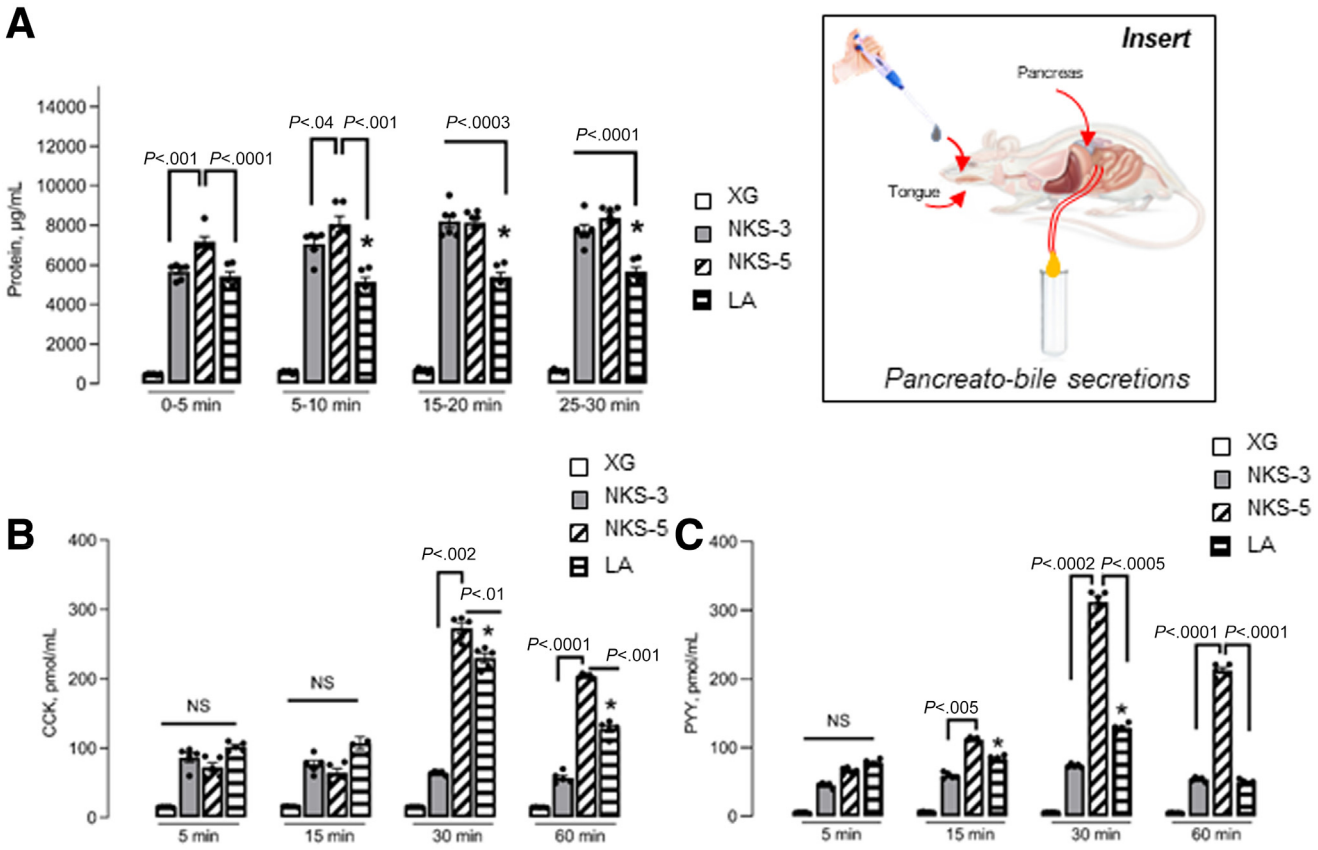

Figure 3. FTA activate tongue-gut loop. (*A*) Effect of lingual application of different agents on pancreato-bile (PB) secretion in mice (*insert*). Animals were anesthetized, and esophageal ligation was performed to prevent any ingestion. They were further subjected to tongue (apical region) application of one of the agents (LA, NKS-3, or NKS-5) at 100 μmol/L (0.2 mL). Control mice received 0.2 mL water containing xanthan gum (XG) at 0.3% (w/v). The figure shows the protein concentrations in the PB secretions at different time points of post-application. Data are mean ± SEM (n = 6). (*B* and *C*) Effect of lingual application of different agents on secretion of CCK (*B*) and PYY (*C*) according to the same protocol as described in *A* except that the mice were bled at different intervals, mentioned under histograms. Asterisks in *B* show statistically different data between LA- and NKS-3-induced responses ($P < .0003$ at 30 minutes; $P < .0002$ at 60 minutes). Asterisks in *C* show statistically different data between LA- and NKS-3-induced responses ($P < .0005$ at 15 minutes; $P < .0006$ at 30 minutes). Data are mean ± SEM (n = 5). Unpaired two-tailed Student *t* test was used.

into blood circulation (Figure 8*A*–*C*). In intraperitoneal glucose tolerance test (IPGTT), two FTA accelerated the glucose clearance in STD- and HFD-fed mice (Figure 8*D* and *E*). Interestingly, the 2 FTA decreased circulatory proinflammatory factors such as lipopolysaccharide (LPS), tumor necrosis factor (TNF) alpha, and interleukin (IL) 6 in obese mice (Figure 8*F*–*H*). Similarly, high concentrations of triglycerides, low-density lipoprotein cholesterol, and total cholesterol in obese mice were decreased by FTA, with an up-regulation of high-density lipoprotein cholesterol in obese mice (Figure 8*I*–*L*).

FTA Exert Beneficial Effects on Liver and Adipose Tissues in Obese Mice

The CD36 mRNA expression in liver was increased in obese mice, and FTA decreased its expression in HFD-fed mice (Figure 9*A*). The up-regulated mRNA expression of key players of liver metabolism such as sterol-regulatory element-binding transcription factor 1c (SREBP1c), stearoyl-CoA desaturase-1 (SCD1), fatty acid synthase (FAS), and peroxisome proliferator-activated receptor-γ (PPAR-γ) was down-regulated by 2 FTA in HFD-fed mice (Figure 9*B*–*E*). The liver IL1β and TNF-α whose mRNA expression was up-regulated in obese mice was significantly decreased by 2 FTA in HFD-fed mice (Figure 9*F* and *G*). The FTA decreased liver weight and concentrations of liver enzymes aspartate aminotransferase and alanine aminotransferase in HFD-fed mice (Figure 9*H*–*J*). Increased size of hepatocytes in obese mice was further decreased by NKS-5, but not NKS-3, in HFD-fed mice (Figure 9*K*). The histologic examination of liver shows the signs of steatosis (marked by the arrows) as microvesicular vacuoles, which are characterized by small, round, and clear vacuoles within the cytoplasm of hepatocytes (Figure 10*A*). In Oil Red staining (Figure 10*B*), inserts show high magnification of respective images. The arrows show the lipid droplets, a marked feature of liver steatosis. The FTA did not influence the liver morphology in STD-fed control mice.

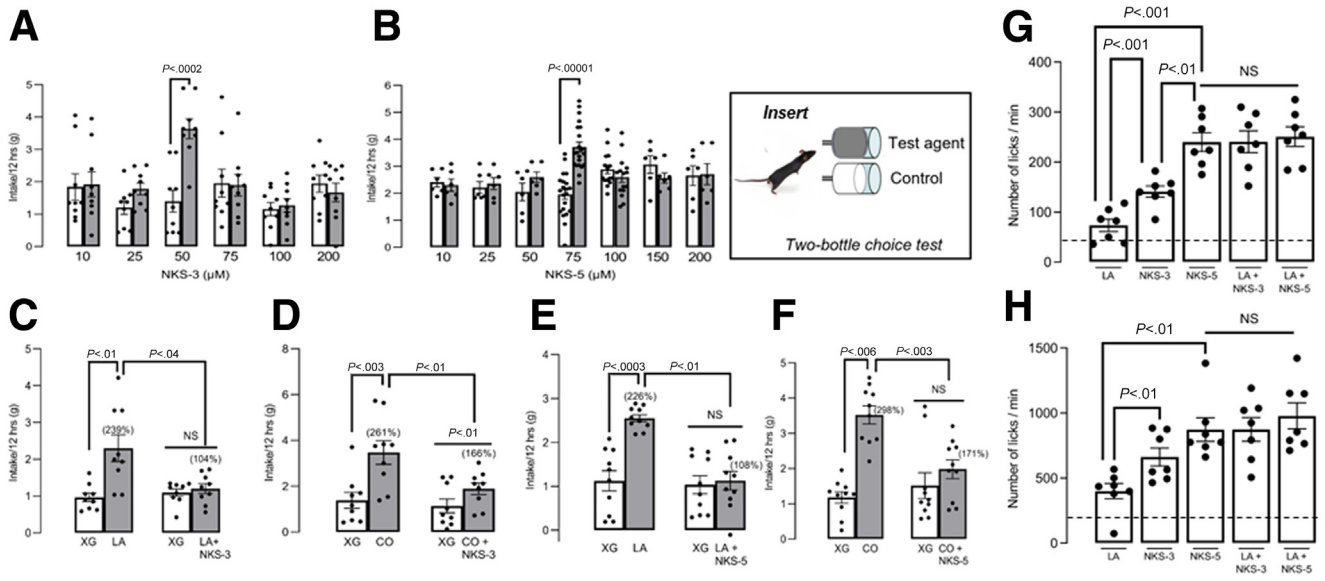

Figure 4. Mice exhibit spontaneous preference for FTA. In 2-bottle choice paradigm (*insert*), mice were subjected to choose between control solution or NKS-3 (*A*) or NKS-5 (*B*) solutions at increasing concentrations. *Open and filled histograms* show the intake of solutions: control (xanthan gum [XG], at 0.3%, w/v) or test, ie, NKS-3 or NKS-5 (in 0.3% XG), respectively. (*C–F*) Effect of addition of NKS-3 at 50 μmol/L (*C*, *D*) or NKS-5 at 75 μmol/L (*E*, *F*) on the preference for LA at 7.4 mmol/L (*C*, *E*) or colza oil (CO) at 0.2%, v/v (*D*, *F*). Data are mean ± SEM (n = 9 in *A*; n = 6 in *B*, except the 75 μmol/L and 100 μmol/L concentrations that included n = 21 and n = 15 animals, respectively. The number of animals in *C* and *D* were n = 9 and in *E* and *F* were n = 10. *Values in brackets* over histograms (*C–F*) show percentage intake of a solution compared with corresponding control (considered as 100%). (*G* and *H*) Licking experiments. After fasting for 6 hours, mice had a brief access (1 or 5 minutes) for solutions containing 0.3% xanthan gum (control solution) or FTA (NKS-3 at 50 μmol/L or NKS-5 at 75 μmol/L) with or without LA (7.4 mmol/L) in a contact lickometer (Med Associates, St Albans, VT) for 1 minute (*G*) or 5 minutes (*H*). *Dotted line* shows the licks evoked by the vehicle solution. Values are means ± SEM, n = 7. Unpaired two-tailed Student *t* test was used.

The mRNA encoding leptin, CD36, TNF-α, and IL6 were up-regulated in obese adipose tissues, and NKS-3 and NKS-5 down-regulated their expression in HFD-fed mice (Figure 11*A*, *C–E*). Interestingly, the adiponectin mRNA expression was up-regulated by FTA in HFD-fed mice (Figure 11*B*). The FTA failed to decrease the size of adipocytes in HFD-fed animals (Figure 11*F*). The adipocytes of obese animals exhibited "crown"-like structures that were decreased after NKS-5 and NKS-3 treatment (Figure 11*G*).

FTA Do Not Exert Genotoxic, Mutagenic, and Endocrine Perturbator Activities

To assess genotoxic property, the micronucleus assays were performed. First, we assessed the cell toxicity of NKS-3 (Tables 3–5) and NKS-5 (Tables 6–8). As regards short treatment in the absence of S9 mix, after the NKS-3 treatments, evidence of toxicity was observed at concentrations ≥0.25 mmol/L. Thus, the maximum concentration of 0.1 mmol/L was selected for determination of induction of micronuclei (Tables 3 and 9). For NKS-5, the maximum concentration of 10 mmol/L was selected for determination of induction of micronuclei (Table 10). The mean frequency of binucleate cells with micronuclei in vehicle control cultures fell within the negative control range. Treatment of cells with each test agent concentration resulted in the frequencies of cells with micronuclei that were similar to those observed in control cultures and fell inside the normal range. The positive control compound (mitomycin C) caused significant increases in the number of binucleate cells containing micronuclei, demonstrating the sensitivity of the test system to detect clastogenic damage.

As regards short treatment in the presence of S9 mix, evidence of NKS-3 toxicity was observed at concentrations ≥0.25 mmol/L. Thus, the maximum concentration of 0.1 mol/L was selected for determination of induction of micronuclei (Tables 4 and 11). For NKS-5, the maximum concentration of 10 mmol/L was selected for determination of induction of micronuclei (Table 12). The mean frequency of binucleate cells with micronuclei in vehicle control cultures fell within the negative control range. Treatment of cells with each test article concentration resulted in the frequencies of cells with micronuclei that were similar to those observed in control cultures. The positive control compound (cyclophosphamide) caused significant increases in the number of binucleate cells containing micronuclei, demonstrating the efficacy of the S9 mix and the sensitivity of the test system (Tables 11 and 12).

After the extended treatment in the absence of S9 mix, evidence of toxicity was observed at concentrations ≥0.03 mmol/L. Thus, the NKS-3 maximum concentration of 0.02 mmol/L was selected for determination of induction of

Table 1. Composition of the Diets

	Normal diet		High-fat diet	
Composition/ingredients	g	Kcal	g	Kcal
Carbohydrate	52.00	208	35.43	141.73
Protein	21.40	85.6	14.58	58.33
Lipids	5.10	45.9	35.34	318.02
Fibers	4	8	2.73	5.45
Minerals ash	5.40	0	3.68	0
Water	12.10	0	8.24	0
Total	100	347.5	100	523.52

NOTE. The different ingredients of the diet are shown as g/100 g.

micronuclei (Table 13). For NKS-5, the maximum concentration of 10 mmol/L was selected for determination of induction of micronuclei (Table 14). The mean frequency of binucleate cells with micronuclei in vehicle control cultures fell within the negative control range. Treatment of cells with each FTA resulted in the frequencies of cells with micronuclei that were similar to those observed in control cultures and fell inside the normal range. The positive control chemicals (vinblastine) caused significant increases in the proportion of binucleate cells with micronuclei, demonstrating the sensitivity of the test system to detect aneugenic damage. It is concluded that NKS-3 and NKS-5 under the conditions of this study did not show any evidence of causing an increase in the induction of micronuclei in human HepG2 cells.

To assess the mutagenic property, *Salmonella-Escherichia coli/*Mammalian Microsome Reverse Mutation Assay was used. NKS-3 was assayed for mutagenic activity in the bacterial reverse mutation test using *S typhimurium* tester strains TA98, TA100, TA1535, and TA1537 and *E coli* tester strain WP2*uvrA(*pKM101) in the presence and absence of phenobarbital/5,6-benzoflavone-induced rat liver S9. The direct plate incorporation method with 48-hour exposure was performed. The doses tested in the mutagenicity assay with all tester strains in both the presence and absence of S9 mix were 50, 150, 500, 1500, and 5000 μg per plate for NKS-3 and 10.0, 33.3, 100, 333, 1000, and 5000 μg per plate for NKS-5. No toxicity was observed in the tester strains at all doses with and without S9. A trouble was observed up to 150 μg per plate for NKS-3 and 330 μg per plate for NKS-5. NKS-3 or NKS-5 did not cause a positive increase in the mean number of revertant per plate with any of the tester strains in either the presence or absence of microsomal enzymes. It is concluded that NKS-3 did not induce mutation in 5 tester strains: TA98, TA100, TA1535, TA1537, and WP2*uvrA(*pKM101), when tested under the conditions of this study in the absence or presence of a rat liver metabolic activation system (S9).

To assess the estrogenic and androgenic agonist/antagonist activity, Hela-9903 cells were exposed to NKS-3 or NKS-5 from 1 nmol/L to 1 mmol/L in dimethyl sulfoxide (0.1% final concentration). In androgen receptor transcriptional activation and inhibition assays, MDA-kb2 cells cultured in vitro were exposed to NKS-3 at 9 concentrations between 1 nmol/L and 1 mmol/L in dimethyl sulfoxide (0.1% final concentration). When tested at concentrations $\geq$10 μmol/L, NKS-3 was cytotoxic for the Hela-9903 and MDA-kb2 cells. Thus, NKS-3 was evaluated to the highest non-cytotoxic concentration of 5 μmol/L in the estrogen receptor and androgen receptor assays. NKS-5 was tested up to the limit concentration of 1 mmol/L in the estrogen receptor and androgen receptor assays. The positive control and reference chemicals induced the appropriate responses. The RPC_{max} (maximum level of response induced by test chemical, expressed as a percentage of the response induced by 1 nmol/L E2) was $<$10% in both assays. The FTA were negative for estrogen receptor transcriptional activation. The RIC_{max} (maximum level of luciferase activity inhibited by test chemical, expressed as a percentage of the response induced by 0.025 nmol/L E2) was $<$30% in both assays. Again, the FTA were negative for estrogen receptor transcriptional inhibition. The RPC_{max} (maximum level of response induced by test chemical, expressed as a percentage of the response induced by 1 nmol/L DHT) was $<$10% in both assays. The FTA were found to be negative for androgen receptor transcriptional activation. The RIC_{max} (maximum level of luciferase activity inhibited by test chemical, expressed as a percentage of the response induced by 0.25 nmol/L DHT) was $<$30% in both assays. The 2 FTA were negative for androgen receptor transcriptional inhibition. It is concluded that NKS-3 and NKS-5 did not exert an estrogenic or antiestrogenic potential. Similarly, NKS-3 and NKS-5 did not possess androgenic or antiandrogenic property.

Toxicological, Conditioned Taste Aversion and Pharmacokinetic Assays of FTA

We performed toxicity tests in rats according to OECD guidelines (425/Dec 2001). The animals showed no clinical signs, discomfort, or mortality. No toxic effect was observed in liver enzymes and blood lipid parameters (Figure 12*A*). Moreover, there were no modifications in the weight of the organs of animals administered NKS-3 or NKS-5 (Table 15).

To further assess the effect of any gastrointestinal pain that could have been caused by the ingestion of FTA, we

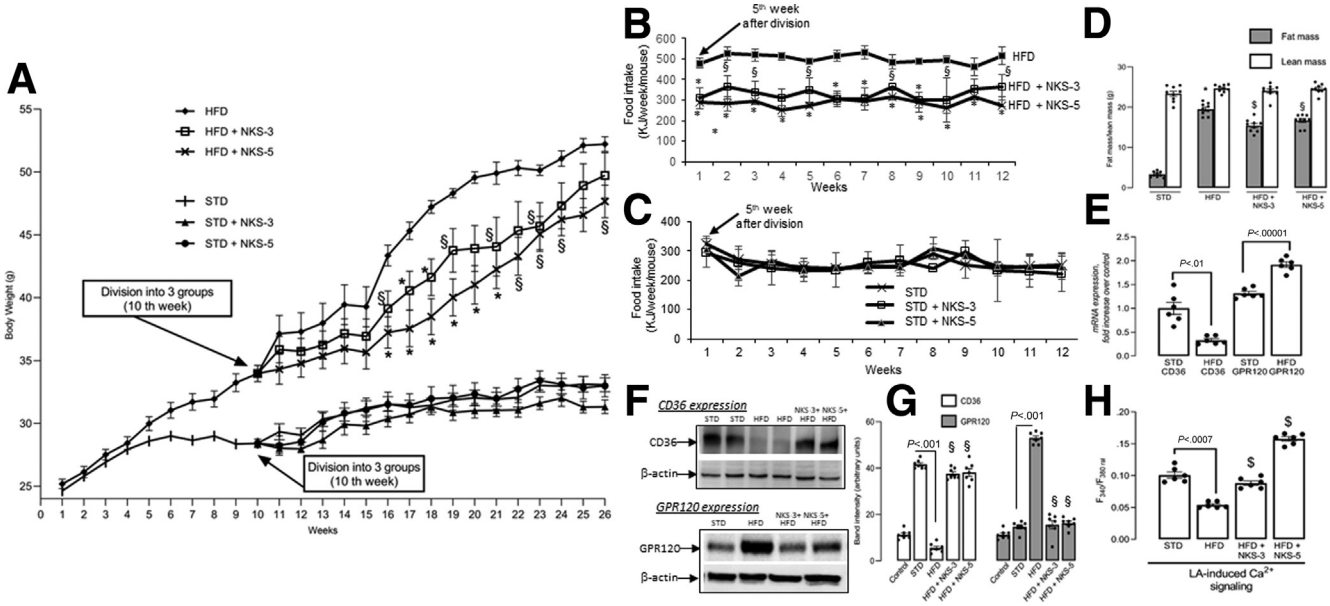

Figure 5. FTA curtail food intake and obesity. The 2-month-old male C57BL/6 mice were fed ad libitum the STD (n = 18) or HFD (n = 18). On week 10, the mice were divided into 6 groups: HFD (n = 6), HFD + NKS-3 (n = 6), HFD + NKS-5 (n = 6), STD (n = 6), STD + NKS-3 (n = 6), and STD + NKS-5 (n = 6). NKS-3 (50 μmol/L) and NKS-5 (75 μmol/L) were added into water bottles for additional 16 weeks (*A*). Control group received water/xanthan gum (0.3%, w/v). *Arrows* (in *A*) indicate week 10 of post-diet feeding when mice were divided into different subgroups and subjected to water bottles containing (or not) FTA. (*B* and *C*) Changes in food intake in different groups from week 5 onward of providing (or not) FTA in water bottles. Data are mean ± SEM. Statistical significance between groups (HFD vs HFD + NKS-3 or HFD + NKS-5) was analyzed by two-way analysis of variance, followed by Tukey multiple comparison test, $^{*}P < .001$; $^{\S}P < .05$. There were no statistical differences in food intake between STD vs STD + NKS-3 or STD + NKS-5 groups (*C*). After 25 weeks of feeding, body lean and fat mass were analyzed by EchoMRI in *D* (fat mass comparison; $^{*}P > .0001$ compared with STD group; $^{\S}P < .0001$, $^{\$}P < .003$, compared with HFD group alone, n = 9). (*E*) Expression of mRNA encoding CD36 and GPR120 in TBC of STD- or HFD-fed mice for 26 weeks (n = 6). (*F*) Representative CD36 and GPR120 protein expression by Western blots in TBC from STD, HFD, and HFD mice that received FTA (NKS-3 or NKS-5) for 16 weeks. (*G*) Densitometric analysis of Western blots of *F* where control is β-actin. §Significant data ($P < .0001$, n = 6), compared with HFD-fed animals. (*H*) LA-induced Ca^{2+} signaling in TBC from mice fed either STD or HFD and maintained or not on NKS-3 and NKS-5 for 16 weeks (n = 6); $^{\$}P < .0001$, compared with HFD group. Data are mean ± SEM. Unpaired two-tailed Student *t* test was used.

conducted classical conditioned taste aversion (CTA) assay. Figure 12*B* shows that although the mice were intraperitoneally injected with LiCl after LA or NKS-3 or NKS-5 intake, they exhibited an aversive behavior on the following day in a short 2-bottle paradigm. However, the NaCl administration after NKS-3 or NKS-5 intake did not show any aversive responses to either of the agents tested.

We further proceeded to analyze the pharmacokinetic properties. To detect the FTA in blood circulation, we used liquid chromatography-mass spectroscopy technique (Figure 13*A* and *B*). The 2 FTA could not be detected in blood circulation of mice after 16 weeks of intake in water bottles. We further performed intravenous injections, and again NKS-5 was below the level of detection, although NKS-3 could be detected in such experimental conditions. For NSK-3, mean concentrations time-course for clearance are mentioned in Figure 13*C*. Pharmacokinetic parameters for NKS-3 are relatively consistent between animals (Table 16). C_{max} is about 48 mg/kg body weight/L for a dose of 10 mg/kg body weight. Mean exposure between the first and the last measurements (area under the curve $[AUC]_{last}$) was close to 60 mg/kg/Lxh and represented about 80% of the total exposure. Clearance was low, leading to a median terminal half-life of 4 hours. The goodness-of-fit plots show a very good correlation between observed and predicted concentrations for the population pharmacokinetic analysis, when NSK-3 concentrations are assumed to follow a bicompartmental model. Because of the limited amount of data, interindividual variability was not estimated for all the parameters; however, the major variability was linked to the intercompartmental clearance, ie, distribution of the drug (Table 17).

Discussion

We have mentioned before that a dysfunction of fat taste receptors, particularly of CD36, in tongue papillae is one of the hallmarks of increased fat detection thresholds that contribute to high fat intake in obese subjects.[14–18] In addition, the dietary fatty acids are less active to trigger satiation than dietary proteins.[24] Therefore, we were interested in synthesizing chemical compounds that could

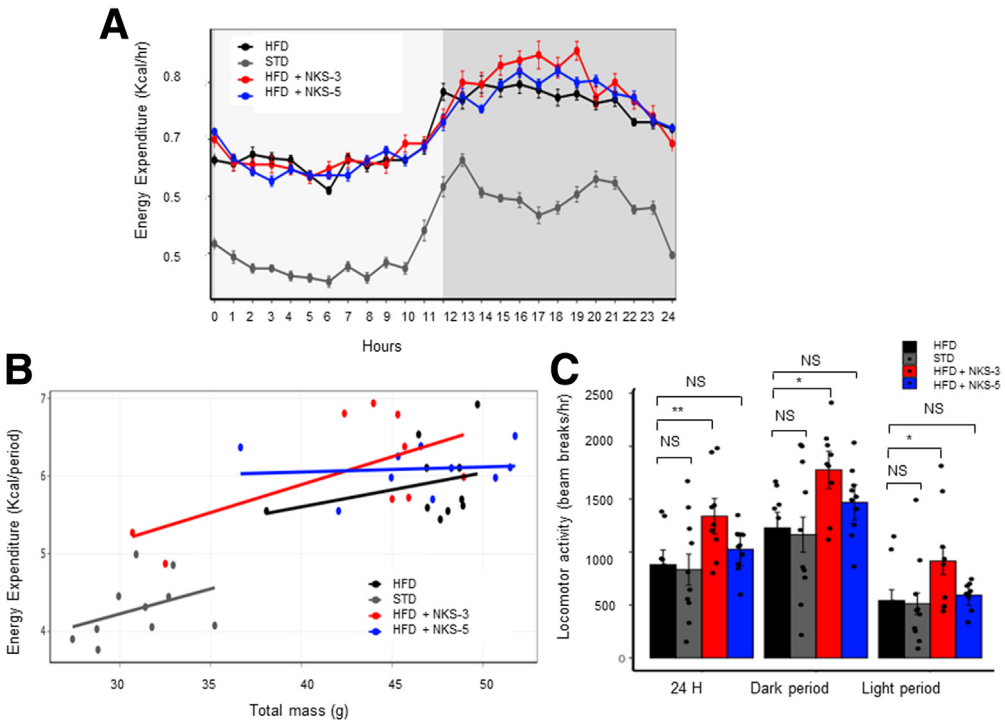

Figure 6. FTA modulate energy balance. Before 4 days of death, the mice were transferred to calorimetric cages. Energy expenditure was determined as mentioned in the Methods for the last 24 hours. (*A*) Whole-body energy expenditure monitored for 24 hours (kcal/h), whereas (*B*) shows regression plot of averaged energy expenditure and total body weight from each mouse. (*C*) Mean values of locomotor activity for full day, dark and light periods (beam breaks/h). Two-way analysis of variance with interaction (analysis of covariance for non-parallel slopes) (*B*) or two-way analysis (C) was used for statistical analysis. $^{*}P \leq .05$; $^{**}P \leq .01$; $^{***}P \leq .001$. Data are represented as mean ± SEM. NS represents insignificant differences. n = 9–10 per group of animals.

trigger high orogustatory perception via lingual CD36 and GPR120 and early satiation that might result in decreased intake of fat-rich food. This kind of approach has been previously adopted by Godinot et al,[25] who used commercially available GPR120 agonists that failed to show any preference in 2-bottle choice tests in the mouse. Cornall et al[26] have also stressed that fat receptors can be the target of obesity and metabolic diseases. These authors demonstrated that a HFD induced up-regulation of GPR43 and GPR120 in a tissue-specific manner.[27] In the present report, we synthesized two (NKS-3 and NKS-5) novel LA derivatives, termed as FTA, to target lingual CD36 and GPR120 to activate tongue-gut loop. We replaced the CO_2H function of LA by 3-oxetan-3-ylmethyl carboxylate or diethyl phosphonate group, respectively, in NKS-5 and NKS-3 compounds. In silico docking studies demonstrate that NKS-3 and NKS-5 exhibited high binding affinities for both CD36 and GPR120, and NKS-5 is superior to LA and NKS-3 in its binding propensity. The interaction of FTA, according to simulations, was found to bind to a number of amino acid residues in CD36 and GPR120.

In human and mouse TBC, NKS-3 triggered a rapid increase in $[Ca^{2+}]i$ via its action on CD36, whereas NKS-5 was found to be an agonist of both CD36 and GPR120. It is noteworthy that FTA-induced Ca^{2+} signaling was higher than that induced by LA. The orosensory perception of a tastant is relayed to brain via nucleus of solitary tract as an afferent electrical response by glossopharyngeal and CT nerves.[5] The FTA-triggered CT nerve responses were higher than those induced by dietary LCFAs such as LA or OA, again

Table 2. Statistical Analysis (*P* Values) of Energy Expenditure

Analyzed groups	Full day	Light period	Dark period
HFD vs STD	0.1075	0.007	0.5003
HFD vs HFD + NKS-3	0.0185	0.06	0.0123
HFD vs HFD + NKS-5	0.6351	0.8347	0.542

NOTE. Values are compared as mentioned in Figure 6*A*. Statistical analyses were performed by two-way analysis of variance with interaction (analysis of covariance for non-parallel slopes), followed by two-tailed Tukey post hoc test.

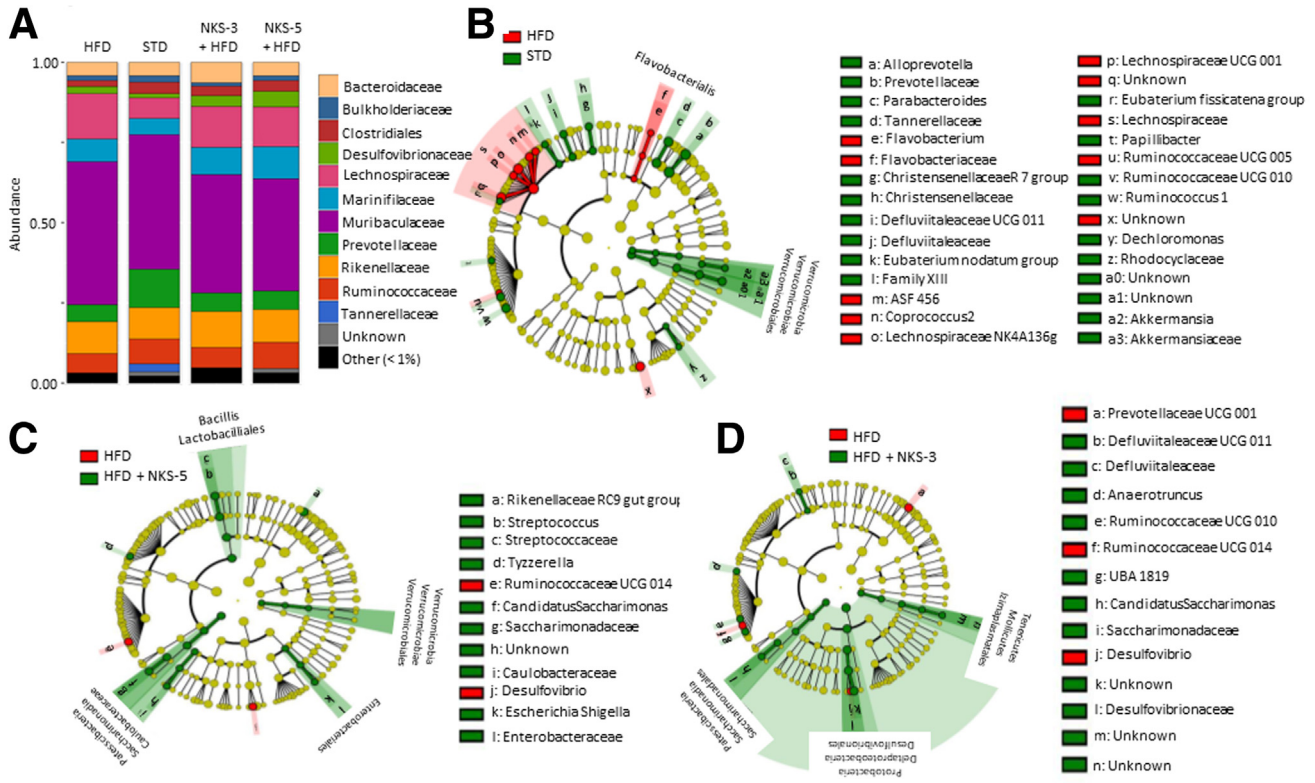

Figure 7. FTA modulate gut microbiota. At end of week 26 of regimen, the mice were killed, and fecal samples (colon) were collected (n = 6 per group of mice). The genomic DNA was extracted and analyzed for bacterial composition by pyrosequencing of the bacterial 16S rRNA fragments as described in the Methods. Results are shown as relative proportion of the taxa at the family taxonomic level (*A*) and the linear discriminant analysis effect size (LefSe) cladograms (*B–D*). Cladograms have been modified from the original output so that all taxonomic names can be read. The biomarkers found by LEfSe are highlighted (*red and green* for pairwise analysis), with the class (group) having the highest median. LEfSe analysis was performed on the complete sequence data (no OTU threshold) for the following groupings: STD vs HFD (*B*), HFD vs HFD + NKS-5 (*C*), and HFD vs HFD + NKS-3 (*D*).

suggesting that FTA are better gustatory signal transducers than LCFA. Furthermore, the addition of FTA to LCFAs (OA and LA) potentiated the CT nerve recordings, again indicating that FTA do not lose their capacity to trigger the gustatory message even in the presence of dietary lipids.

The binding of a dietary LCFA and a GPR120 agonist such as TUG891 to lingual taste receptors has been reported to activate tongue-brain-gut loop,[1,28] which is responsible for the anticipatory physiological mechanisms such the secretion of PB juice. NKS-5 was more potent than LCFA on PB secretion, although NKS-3 was better than LCFA from 5 minutes onward. In the same experimental set-up, NKS-5 was more potent inducer of the release of CCK and PYY into blood circulation. The kinetics of the secretion of PB and gut peptides do not overlap with each other because the secretion of the former was immediately recuperated by a catheter, whereas the release of gut peptides into blood took a little more time.

Rodents exhibit a spontaneous preference for dietary LCFAs.[5,7,8] In a 2-bottle paradigm, mice exhibited a gustatory preference for NKS-3 (at 50 μmol/L), NKS-5 (at 75 μmol/L), and LA (previously used at 7.4 mmol/L).[3] These observations suggest that NKS-3 and NKS-5 might be 142 and 95 times more potent, respectively, than a natural LCFA to trigger a gustatory attraction. Nonetheless, the FTA lost their gustatory property at high concentrations, which may be due to receptor down-regulation, or alternatively, their intense fat taste (at high concentration) will not be preferred any more as has been reported in human participants who do not prefer fatty acids at high concentrations.[29] Indeed, it has been reported previously that fat taste varies and may become from pleasant to unpleasant, according to the concentrations of fatty acids and oily mixtures.[29] Similarly, the combined mixture (FTA plus fatty acids/oil) might have resulted in an unpalatable fat taste that would be no more hedonic for mice, although the FTA still retained their high intrinsic capacity to send strong gustatory message to brain because we have mentioned before that FTA (even at high concentrations) in the presence of dietary LCFAs induced an additive CT nerve response and also did not decrease licking responses to LCFA. We further ascertained whether FTA, similarly, might interfere with the ingestion of fat-rich food. Generally, in most of the protocols, the animals are given an anti-obesity agent before feeding the HFD. However, we wanted to assess the interventional effect of novel FTA on the

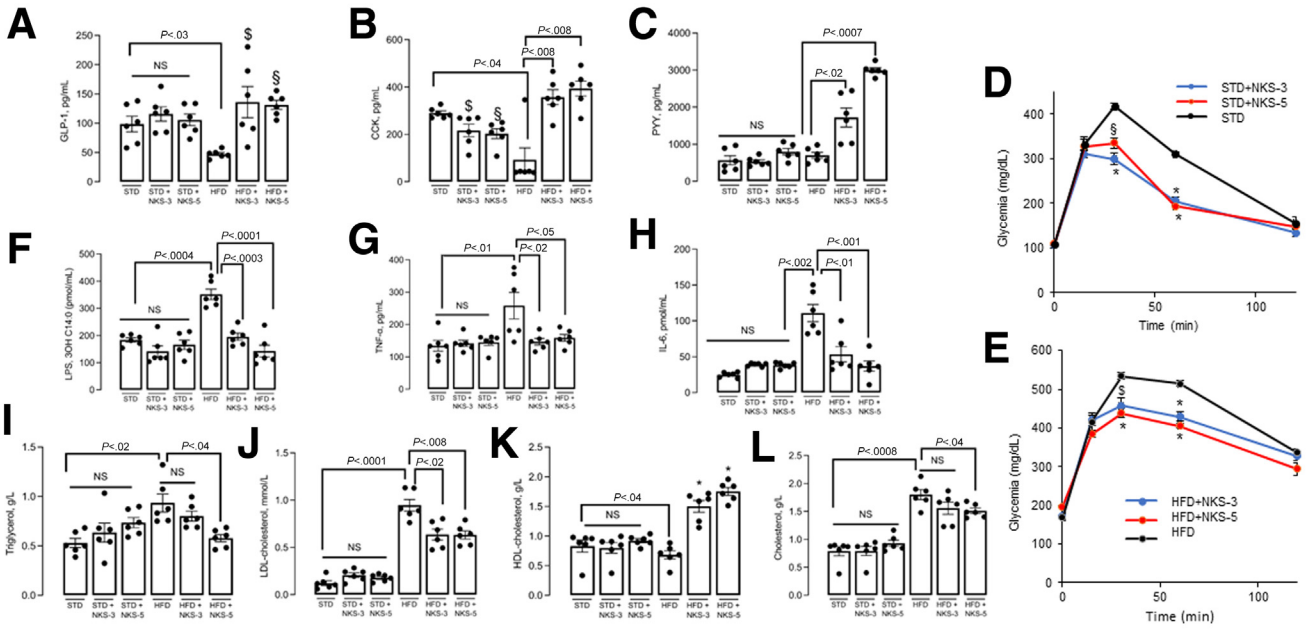

Figure 8. FTA trigger release of gut peptides and modulate insulin resistance, inflammation, and dyslipidemia. At end of week 26 of regimen, mice were killed, and blood was withdrawn by a vacutainer to determine GLP-1 (*A*, $^{\$}P < .03$, $^{\S}P < .003$, compared with HFD group); CCK (*B*, $^{\$}P < .04$, $^{\S}P < .03$, compared with STD group (*B*); PYY (*C*), LPS (*F*), TNF-α (*G*), IL-6 (*H*), triglycerol (*I*), low-density lipoprotein cholesterol (*J*), high-density lipoprotein cholesterol (*K*), $^{*}P < .001$ compared with HFD group (*K*), and cholesterol (*L*) (n = 6). Unpaired two-tailed Student *t* test was used. NS, insignificant differences between the compared groups. IPGTT was performed (*D* and *E*). Data are mean ± SEM (n = 6). Statistical significance compared with the control group time points was analyzed by two-way analysis of variance, followed by Tukey multiple comparison test, $^{*}P < .001$; $^{\S}P < .01$.

ingestion of a fat-rich food in already "installed obesity". Although NKS-5 was more potent than NKS-3, both the FTA decreased food intake and weight gain and fat mass, but not lean mass, in obese mice. Indirect calorimetry showed that NKS-3, but not NKS-5, promoted a high metabolic rate by increasing energy expenditure. This observation could be the consequence of a high locomotor activity shown in the NKS-3 group during both the night and the day. Interestingly, the down-regulated LA-induced TBC Ca^{2+} signaling in obese mice[3] was up-regulated by FTA, and it was correlated with up-regulation of CD36 protein after weight loss in FTA-administered obese mice. The up-regulation of FTA-triggered Ca^{2+} signaling may contribute to their actions in obesity. However, a decrease in body weight may also involve the post-ingestive hormonal effects of FTA. After dietary fats are emulsified/processed through the action of lipases and bile acids, they are transported into enterocytes by a number of proteins such as FABP and CD36. The gastrointestinal tract is heavily innervated by both vagal and dorsal root afferents. By using post-oral conditioning of mice, Berthoud et al[30] have demonstrated that intestinal fatty acid sensing activates gut-brain loop including reward systems through CCK-sensitive vagal afferent fibers passing through the right nodose ganglion. Ogawa et al[31] have demonstrated that direct lipid infusion into jejunum decreased fat-rich food intake and dose-dependently increased plasma GLP-1, PYY, and CCK without influencing ghrelin levels, and the anorectic effect involved the activation of gut-brain loop as vagotomy or midbrain transection abolished the changes in fat-rich food intake. We also observed high blood concentrations of GLP-1 and CCK in obese mice that received NKS-3 or NKS-5. CCK, secreted by neuroendocrine I cells of small intestine, decreases gastric emptying and induces satiety by acting on its receptors in brain and vagus nerve.[32] The CCK type-1 receptors have been the target of anti-obesity strategies.[33] GLP-1 is released primarily by L-type cells of the ileum in response to nutrient ingestion and has been reported to induce moderate weight loss in diabetic subjects.[31] In addition, FTA also increased the concentrations of anorectic PYY, which has been shown to be co-released with GLP-1 by L-type cells.[34]

It has been well-demonstrated that a balance between gut microbes (Bacteroidetes and Firmicutes) is critically involved in the pathogenesis of obesity, where the former exerts a beneficial effect, and the latter promotes/aggravates obesity.[35] We observed that obese mice had high number of bacteria that belonged to Lachnospiraceae family, which is part of the Firmicutes phylum. These bacteria are known to contribute to the development of obesity through high intestinal absorption of dietary energy.[36] The gut microbiota of STD-fed mice was dominated by beneficial Akkermensiaceae bacteria.[37] Indeed, *A muciniphila* has been shown to attenuate diet-induced obesity and to restore gut barrier dysfunction in mouse models.[35] NKS-3 shifted the microbial population to a large unknown phylum of

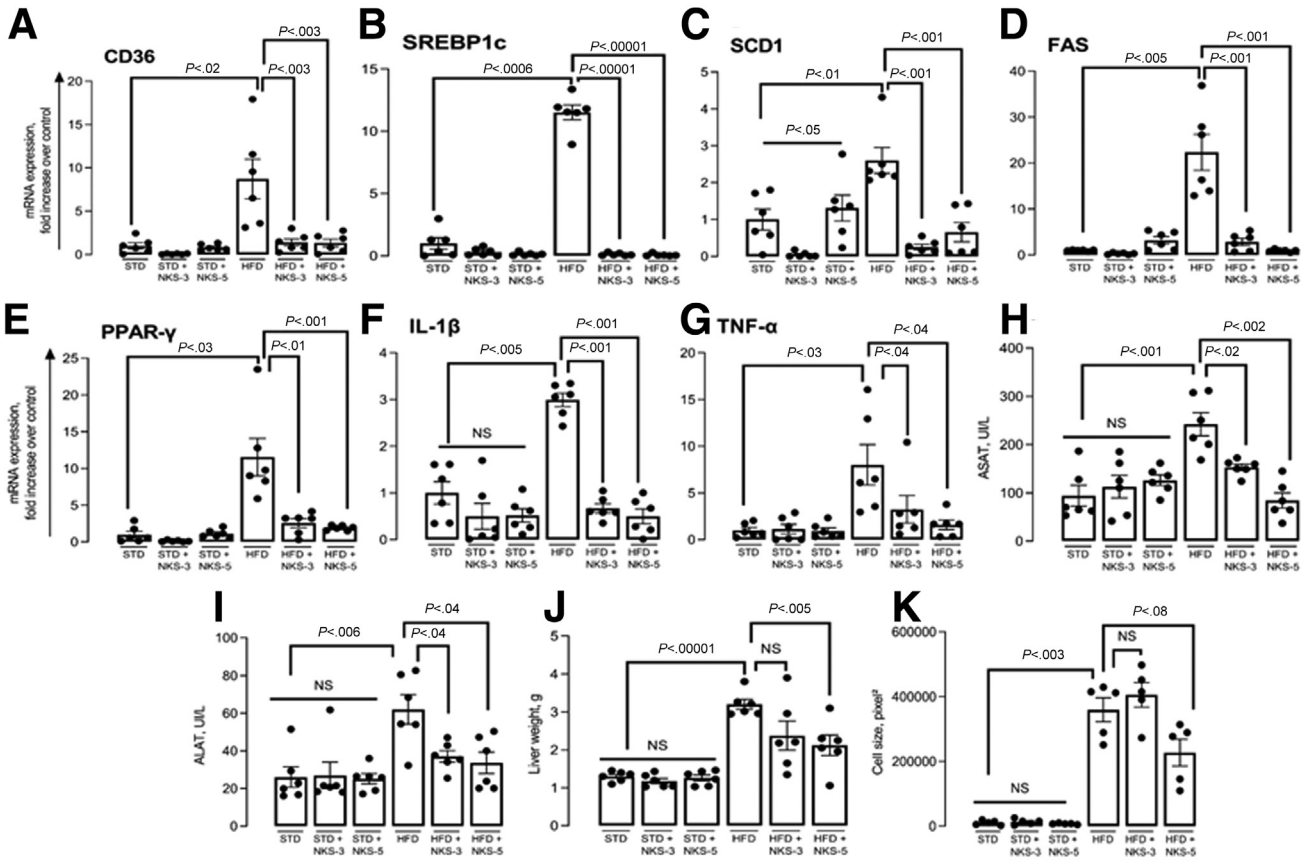

Figure 9. FTA improve liver functions. After death the liver was weighed and used for the expression of mRNA encoding a number of agents involved in liver lipid metabolic pathway and functions, ie, CD36 (*A*), SREBP1c (*B*), SCD1 (*C*), FAS (*D*), PPAR-γ (*E*), IL-1β (*F*), and TNF-α (*G*). The activity of liver enzymes, ie, aspartate aminotransferase (ASAT) (*H*) and alanine aminotransferase (ALAT) (*I*), and liver weight (*J*) and size of hepatocytes (in 5-μm-thick/hematoxylin-eosin colored sections) (*K*) were also determined. Data are mean ± SEM, n = 6 (*A*–*J*) or n = 5 (*K*). Unpaired two-tailed Student *t* test was used. NS, insignificant differences.

bacteria; nonetheless, it decreased the Lachnospiraceae bacteria that were high in HFD-fed obese mice. Indeed, the Lachnsospraceae have been shown to be high in genetically induced obesity in mice[38] and contribute to liver fibrosis in nonalcoholic fatty liver disease in obese patients.[39] NKS-5 shifted the microbiota population to Patescibacteria phylum as evidenced by high bacteria of Saccharimonadaceae family, whose numbers were decreased in obesity.[40] NKS-5 also increased the number of *Candidatus Saccharimonas* bacteria, which are known to induce an increase in butyrate and propionate production in the gut and, therefore, to reduce inflammation by TNF-α and IL10.[41] This change in gut microbiota by FTA may also contribute to their anti-inflammatory actions. Interestingly, FTA exerted anti-inflammatory action in obese animals by decreasing circulating LPS, IL6, and TNF-α concentrations, although NKS-5 failed to decrease significantly TNF-α levels in obese mice. The dyslipidemia was also normalized as far as triglycerides, low-density lipoprotein cholesterol, high-density lipoprotein cholesterols, and total cholesterol concentrations are concerned.

It has been reported that the HFD up-regulates hepatic CD36 and PPAR-γ mRNA expression that provokes liver steatosis in mice.[42] Hepatic mRNA expression of SREBP1c, FAS, and SCD1 is also up-regulated in obese mice.[42] The FTA decreased the expression of these lipogenic genes in liver of obese mice, demonstrating that the novel lipid analogues may lower hepatic lipid accumulation via SREBP1c-mediated transcription pathway. Aspartate aminotransferase and alanine aminotransferase are widely used as serum enzyme biomarkers of liver injury, and their levels are increased with obesity. Because alanine aminotransferase is the most sensitive biomarker of hepatic steatosis, it is associated with increased abdominal weight and obesity.[43] The histologic examination shows a clear liver steatosis in obese mice, observed by Oil red droplets. Both FTA decreased not only the circulating concentrations of alanine aminotransferase and aspartate aminotransferase but also liver weight in HFD-fed mice, showing that NKS-3 and NKS-5 exert protective effects on liver steatosis. As regards the hepatocyte size, NKS-5 was more potent than NKS-3. Obesity has been shown to lead to hepatocarcinoma by high concentrations of TNF-α and IL1β mRNA.[44] The 2 FTA exerted beneficial effects by decreasing liver mRNA of these 2 proinflammatory markers in obese mice.

Diet-induced obesity is associated with up-regulation of leptin and down-regulation of adiponectin mRNA along with

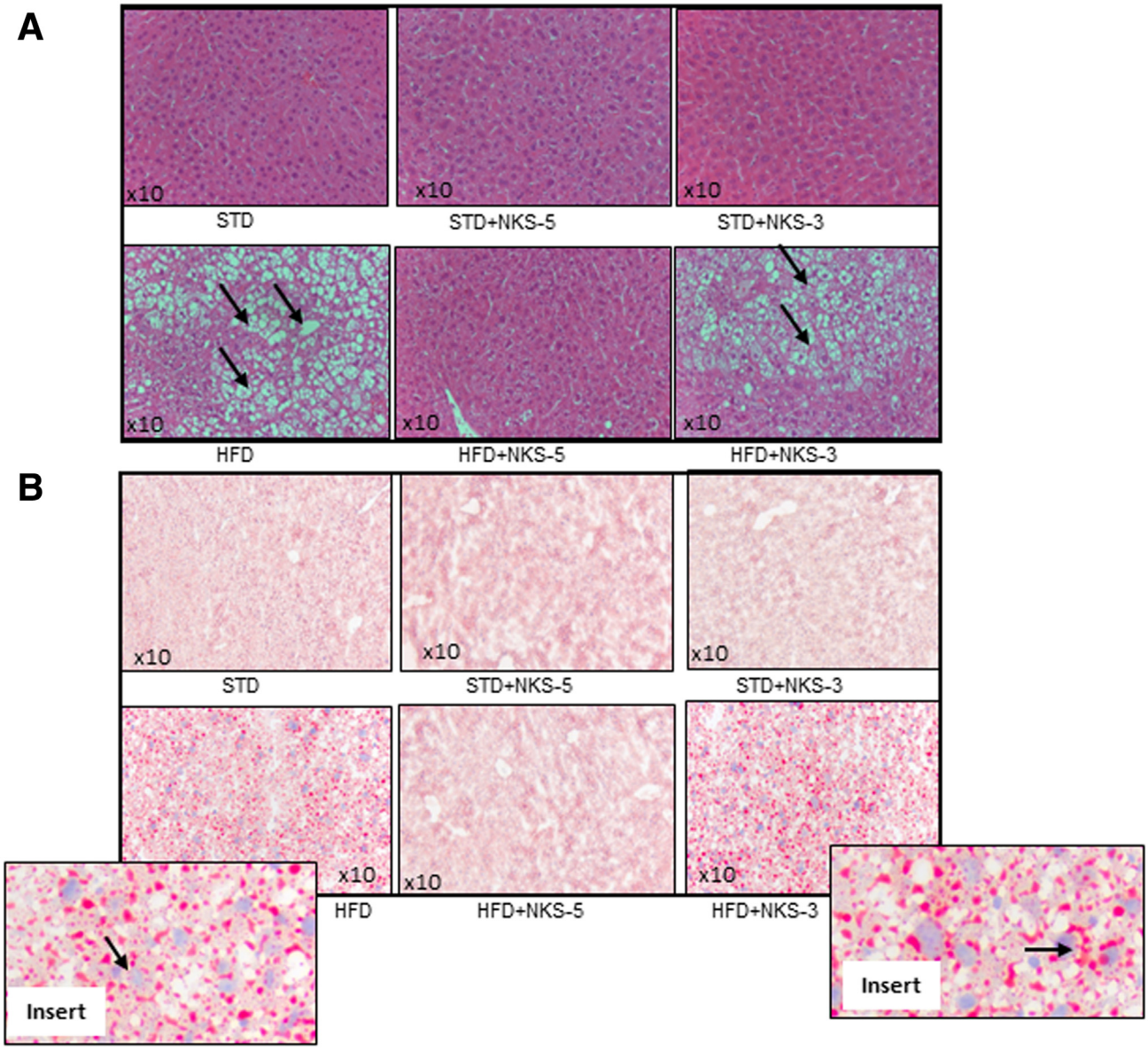

Figure 10. FTA protect against liver steatosis. Histologic analyses of representative liver sections from STD-fed control and HFD-fed obese mice. Animals were maintained on STD or HFD with or without FTA (NKS-3 or NKS-5) for 16 weeks. After death, liver sections of control and obese mice, given NKS-3 or NKS-5 or no treatment, were used for histologic analysis. Representative pictures were obtained by staining with hematoxylin-eosin **(*A*)** and Oil Red **(*B*)** as described in Methods. Original magnification ×10. *Arrows* in *A* show microvesicular vacuoles in hepatocytes. *Insert* shows magnified sections, and *arrows* indicate lipid droplets.

high expression of mRNA encoding proinflammatory cytokines in adipose tissues.[45] The FTA up-regulated adiponectin mRNA and decreased leptin mRNA expression, although NKS-3 failed to significantly decrease the latter in adipose tissues of HFD-fed mice. Leptin is also a proinflammatory adipokine. In addition, we observed that FTA deceased adipocyte hypertrophy (large size), marked with crown-like structures. The increased CD36 mRNA expression in adipose tissues of obese mice was down-regulated by 2 FTA. These observations suggest that FTA exert anti-inflammatory action in adipose tissue.

Last, we report that the FTA exerted no mutagenic, genotoxic, or endocrine disrupter properties. No toxicity was observed while determining median lethal dose in rat model. Lithium chloride administration has been used to induce malaise during the first intake of a tastant or food ingredient to induce the aversive behavior, on the following day, toward the same gustatory cue in rodents.[46] Whether intake of novel FTA may trigger gastric malaise and decrease fat-rich food intake, we performed CTA assays. It is noteworthy that in CTA experiments, the animals received high concentrations of LA (2%) and 2 FTA (5 mmol/L)

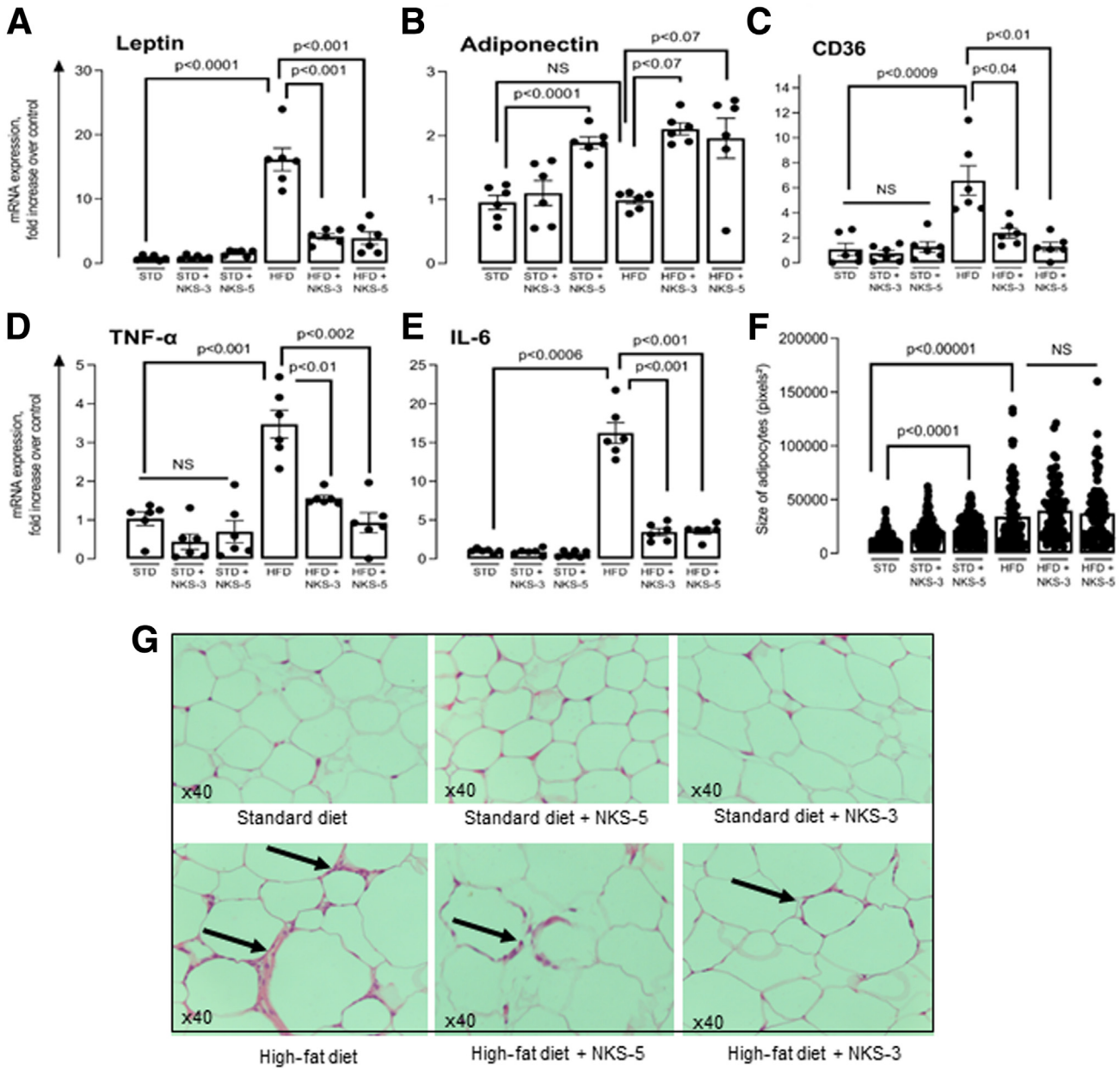

Figure 11. FTA modulate epididymal adipose tissue functions. After death the epididymal adipose tissue was sampled and used for the expression of mRNA coding leptin (*A*), adiponectin (*B*), CD36 (*C*), TNF-α (*D*), and IL-6 (*E*). Size of adipocytes was also measured by microscopic analysis of 5-μm-thick/hematoxylin-eosin colored sections (*F*)**.** Data are mean ± SEM, n = 6 animals (*A–E*) or different *n* observations in (*F*): STD, n =263; STD + NKS-3, n = 156; STD + NKS-5, n = 155; HFD, n = 100; HFD + NKS-3, n = 82; HFD + NKS-5, n = 89. NS, insignificant differences. Unpaired two-tailed Student *t* test was used. (*G*) Histologic analyses of representative epididymal adipose tissue sections from STD-fed control and HFD-fed obese mice. Animals were maintained on a diet for 16 weeks. After death, adipose tissue sections of control and obese mice, given NKS-3 or NKS-5, were used for histologic analysis. Representative pictures were obtained by staining with hematoxylin-eosin. Original magnification ×40. *Arrows* show crown-like structures.

before LiCl or NaCl administration because we wanted to assess whether this dose of the FTA might trigger a malaise (in NaCl group) like LiCl and induce an aversive behavior. This concentration of NKS-3 and NKS-5 is 100 and 66 times higher, respectively, than that used for anti-obesity effects in HFD-fed mice, where NKS-3 and NKS-5 are used at 50 and 75 μmol/L, respectively. We observed that the 2 FTA did not induce an aversive behavior with NaCl administration, although, as expected, LiCl administration triggered CTA with FTA and LA. As far as the pharmacokinetic is concerned, we could not detect FTA in blood circulation even after 16 weeks of intake in water bottles. Nonetheless, we intravenously injected them to determine the pharmacokinetic values. Hence, C_{max} for NKS-3 rapidly reached 48 mg/kg/L for a

Table 3. NKS-3 Cytotoxicity Evaluation: Short Treatment in Absence of S9 Mix

Treatment	Concentration in culture medium	Cells with 1N	Cells with 2N	Cells with >2N	Total number of cells	CBPI	Mean CBPI	Cytotoxicity (%)
Dimethyl sulfoxide	1% (v/v)	165	295	43	503	1.76	1.76	0.00
		143	314	43	500	1.80		
		158	309	35	502	1.75		
		162	307	31	500	1.74		
NKS-3	0.025 mmol/L	130	326	47	503	1.83	1.84	–9.99
		120	341	41	502	1.84		
	0.050 mmol/L	188	298	17	503	1.66	1.65	14.67
		196	290	16	502	1.64		
	0.100 mmol/L	363	139	2	504	1.28	1.33	56.19
		316	179	7	502	1.38		
	0.25 mmol/L	369	131	5	503	1.25	1.26	65.53
		383	116	4	505	1.28		
	0.40 mmol/L	—	—	—	—	—	—	Cell death
	0.50 mmol/L	—	—	—	—	—	—	Cell death
	1.00 mmol/L	—	—	—	—	—	—	Cell death
	5.00 mmol/L	—	—	—	—	—	—	Cell death
	10.00 mmol/L	—	—	—	—	—	—	Cell death
Mitomycin C	0.025 μg/mL	184	286	32	502	1.70	1.70	8.75
		180	294	27	501	1.69		

CBPI, Cytokinesis Block Proliferative Index = [(cells with 1N × 1) + (cells with 2N) + (cells with greater than 2N × 3)] / total cells
% de cytotoxicity = 100 – 100 [(CBPI test article -1) / (CBPI vehicle -1)]; N, nuclei.

dose of 10 mg/kg. The AUC_{last} was equal to 60 mg/kg/L/h and represented about 80% of the total exposure. Clearance was low, leading to a median terminal half-life of 4 hours. Interestingly, NKS-5 could not be detected, even in intravenous administration, in blood circulation, and we failed to perform noncompartmental analysis.

The overall results show that 2 FTA exert beneficial interventional effects during the progression of obesity, and NKS-5 seems to be a better compound than NKS-3. Ours is the first study on targeting fat taste receptors, leading to activation of tongue-gut loop as a therapeutic approach, and it opens new vistas to synthesize more potent chemical compounds to decrease progressive weight gain under HFD consumption. However, further studies are in progress in our laboratory to better understand the mechanisms of action of the FTA on hepatic and intestinal functions and other metabolic pathways in relation with dietary fatty acids.

Table 4. NKS-3 Cytotoxicity Evaluation: Short Treatment in the Presence of S9 Mix

Treatment	Concentration in culture medium	Cells with 1N	Cells with 2N	Cells with >2N	Total number of cells	CBPI	Mean CBPI	Cytotoxicity (%)
Dimethyl sulfoxide	1% (v/v)	141	309	51	501	1.82	1.80	0.00
		142	320	38	500	1.79		
		139	324	37	139	1.80		
		132	336	32	132	1.80		
NKS-3	0.025 mmol/L	114	359	27	500	1.83	1.83	–3.60
		105	372	23	500	1.84		
	0.050 mmol/L	120	349	32	501	1.82	1.84	–5.03
		104	364	34	502	1.86		
	0.100 mmol/L	196	293	12	501	1.63	1.65	19.37
		179	313	9	501	1.66		
	0.25 mmol/L	419	74	14	507	1.20	1.22	73.00
		398	88	14	500	1.23		
	0.40 mmol/L	—	—	—	—	—	—	Cell death
	0.50 mmol/L	—	—	—	—	—	—	Cell death
	1.00 mmol/L	—	—	—	—	—	—	Cell death
	5.00 mmol/L	—	—	—	—	—	—	Cell death
	10.00 mmol/L	—	—	—	—	—	—	Cell death
Cyclophosphamide	5 μg/mL	164	315	29	508	1.73	1.70	13.00
		194	284	24	502	1.66		

CBPI, Cytokinesis Block Proliferative Index = [(cells with 1N × 1) + (cells with 2N) + (cells with greater than 2N × 3)] / total cells
% de cytotoxicity = 100 – 100 [(CBPI test article -1) / (CBPI vehicle -1)]; N, nuclei.

Table 5. NKS-3 Cytotoxicity Evaluation: Extended Treatment in the Absence of S9 Mix

Treatment	Concentration in culture medium	Cells with 1N	Cells with 2N	Cells with >2N	Total number of cells	CBPI	Mean CBPI	Cytotoxicity (%)
Dimethyl sulfoxide	1% (v/v)	105	333	63	501	1.92	1.92	0.00
		92	333	75	500	1.97		
		118	317	65	500	1.89		
		121	314	66	501	1.89		
NKS-3	0.0065 mmol/L	204	277	21	502	1.64	1.69	24.86
		155	319	26	500	1.74		
	0.010 mmol/L	215	263	23	501	1.62	1.59	35.26
		230	255	15	500	1.57		
	0.020 mmol/L	284	201	16	501	1.47	1.46	49.48
		278	215	8	501	1.46		
	0.030 mmol/L	379	121	2	502	1.25	1.25	72.83
	0.040 mmol/L	384	113	4	501	1.24	1.24	73.65
	0.062 mmol/L	—	—	—	—	—	—	Cell death
	0.125 mmol/L	—	—	—	—	—	—	Cell death
Vinblastine	0.0025 μg/mL	232	214	64	510	1.67	1.67	27.05
		233	218	62	513	1.67		

CBPI, Cytokinesis Block Proliferative Index = [(cells with 1N × 1) + (cells with 2N) + (cells with greater than 2N × 3)] / total cells
% de cytotoxicity = 100 – 100 [(CBPI test article -1) / (CBPI vehicle -1)]; N, nuclei.

Materials and Methods

Materials

The culture media (IMDM and RPMI-1640) and L-glutamine were purchased from Lonza Verviers (Belgium). Fura-2/AM was procured from Invitrogen (USA). All other chemicals including MCDB153 medium were from Merck/Sigma (USA). The antibodies for CD36 were from R&D, UK (AF 2519) and those for GPR120 from Santa Cruz, USA (sc-48203). The inhibitors of GPR40 (GW1100; ref. 371830) and GPR43 (GLPG0974; ref. SML2443) were from Merck, USA. Sulfo-N-succinimidyl oleate, SSO (ref. SML2148), and AH-7614 SML2025) were from Merck/Sigma, USA. Anti–beta-actin antibodies (ref. MAB8929) were from Biotechne-R&D Systems, USA. Enhance chemiluminescence (ref. 1705060) was obtained from Biorad, France. All other chemicals, unless specified, including LA (ref. L1376), OA (O1008), and xanthan gum (ref. G1253) were procured from Merck/Sigma (USA).

Animals

We used 2-month-old C57BL/6J male mice, which are generally used for diet-induced obesity.[22] Animals were maintained at a temperature of 22°C ± 3°C, with a relative humidity of 50% ± 20%, and a 12-hour light/dark cycle. Standard laboratory food (A03 rodent diet; Scientific Animal Food and Engineering, Villemoisson-sur-Orge, France) and water were given ad libitum. All experiments on animals were performed as per European guidelines on the protection of animals, and experimental protocol (no. 16198) was approved by the regional ethical committee of Burgundy University. The mice were anesthetized with 2% isofluorane gas. This method induces a deep sleep without perturbing

Table 6. NKS-5 Cytotoxicity Evaluation: Short Treatment in the Absence of S9 Mix

Treatment	Concentration in culture medium	Cells with 1N	Cells with 2N	Cells with >2N	Total number of cells	CBPI	Mean CBPI	Cytotoxicity (%)
Dimethyl sulfoxide	1% (v/v)	110	332	60	502	1.90	1.93	0.00
		101	341	60	502	1.92		
		100	327	73	500	1.95		
		115	294	93	502	1.96		
NKS-5	2.5 mmol/L	79	352	69	500	1.99	1.98	–5.78
		76	355	70	501	1.98		
	5 mmol/L	95	347	64	506	1.94	1.94	–1.42
		84	360	58	502	1.95		
	10 mmol/L	117	313	70	500	1.91	1.92	1.32
		108	333	72	513	1.93		
Mitomycin C	0.05 μg/mL	244	234	23	501	1.56	1.54	41.48
		244	250	8	502	1.53		

CBPI, Cytokinesis Block Proliferative Index = [(cells with 1N × 1) + (cells with 2N) + (cells with greater than 2N × 3)] / total cells
% de cytotoxicity = 100 – 100 [(CBPI test article -1) / (CBPI vehicle -1)]; N, nuclei.

Table 7. NKS-5 Cytotoxicity Evaluation: Short Treatment in the Presence of S9 Mix

Treatment	Concentration in culture medium	Cells with 1N	Cells with 2N	Cells with >2N	Total number of cells	CBPI	Mean CBPI	Cytotoxicity (%)
Dimethyl sulfoxide	1% (v/v)	95	303	102	500	2.01	2.06	0.00
		68	326	106	500	2.08		
		63	340	98	501	2.07		
		60	331	109	500	2.10		
NKS-5	2.5 mmol/L	59	354	87	500	2.07	2.07	–0.59
		68	346	87	501	2.07		
	5 mmol/L	67	393	140	600	2.12	2.13	–6.22
		47	337	117	501	2.14		
	10 mmol/L	61	344	96	501	2.06	2.05	1.64
		78	401	121	600	2.04		
Cyclophosphamide	10 μg/mL	129	279	92	500	1.93	2.01	5.30
		85	285	130	500	2.09		

CBPI, Cytokinesis Block Proliferative Index = [(cells with 1N × 1) + (cells with 2N) + (cells with greater than 2N × 3)] / total cells
% de cytotoxicity = 100 – 100 [(CBPI test article -1) / (CBPI vehicle -1)]; N, nuclei.

the physiological parameters. For the measurements of CT recordings, 2-month-old male C57BL/J6 mice were purchased from Pasteur Institute of Teheran (Iran), and the experimental protocol was approved by the Ethical Committee of Faculty of Medical Sciences, Tarbiat Modares University (Tehran).

Chemical Synthesis

NKS-3 (diethyl (9Z,12Z)-octadeca-9,12-dien-1-ylphosphonate, ie, $C_{22}H_{43}PO_3$) was prepared from LA by using the following design strategy, composed of 3 steps, resulting in the final synthesis:

Hence, $LiAlH_4$ (0.18 g, 4.8 mmol) was suspended in tetrahydrofuran (25 mL) in a round bottom flask. A solution of LA (1.24 mL, 4.0 mmol) in tetrahydrofuran (15 mL) was added dropwise at 0°C. The mixture was slowly warmed up to room temperature (20°C–25°C) and stirred overnight. The mixture was quenched by addition of distilled water (2 mL) and 15% aqueous NaOH (5 mL) and was further diluted in ethanol, transferred into a separating funnel, and then washed with brine. The organic phase was dried over $MgSO_4$. The product was purified by a column chromatography on SiO_2 (petroleum ether/ ethyl acetate (5:1), Rf = 0.80). m_{pure} = 0.96 g. Aspect: colorless oil. Yield: 91%. ^1H

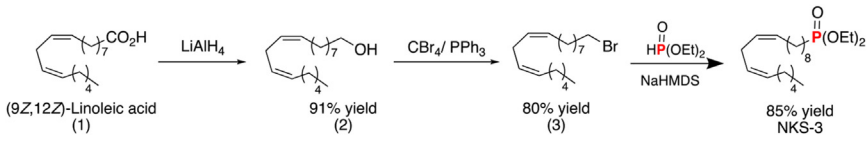

Table 8. NKS-5 Cytotoxicity Evaluation: Extended Treatment in the Absence of S9 Mix

Treatment	Concentration in culture medium	Cells with 1N	Cells with 2N	Cells with >2N	Total number of cells	CBPI	Mean CBPI	Cytotoxicity (%)
Dimethyl sulfoxide	1% (v/v)	84	277	139	500	2.11	2.05	0.00
		104	270	129	503	2.05		
		94	302	104	500	2.02		
		114	269	117	500	2.01		
NKS-5	2.5 mmol/L	103	286	111	500	2.02	1.99	5.29
		119	282	102	503	1.97		
	5 mmol/L	141	292	68	501	1.85	1.84	19.58
		135	318	49	502	1.83		
	10 mmol/L	116	299	89	504	1.95	1.89	14.66
		173	341	78	592	1.84		
Vinblastine	0.025 μg/mL	114	285	101	500	1.97	1.95	9.29
		128	328	87	543	1.92		

CBPI, Cytokinesis Block Proliferative Index = [(cells with 1N × 1) + (cells with 2N) + (cells with greater than 2N × 3)] / total cells
% de cytotoxicity = 100 – 100 [(CBPI test article -1) / (CBPI vehicle -1)]; N, nuclei.

Table 9. Micronucleus Analysis of NKS-3: Short Treatment in the Absence of S9 Mix

Treatment	Concentration in culture medium	Total BN cells scored	Total MNBN cells scored	MNBN cells frequency (%)	Mean frequency (%)
Dimethyl sulfoxide	1% (v/v)	1000	7	0.7	0.70
		1000	7	0.7	
		1000	8	0.8	
		1000	6	0.6	
NKS-3	0.025 mmol/L	1000	6	0.6	0.55
		1000	5	0.5	
	0.05 mmol/L	1000	7	0.7	0.70
		1000	7	0.7	
	0.10 mmol/L	1000	7	0.7	0.65
		1000	6	0.6	
Mitomycin C	0.025 μg/mL	1000	31	3.1	3.25
		1000	34	3.4	

BN, binucleate cells; MNBN, micronucleated binucleate cells.

NMR (500 MHz, $CDCl_3$) δ (ppm): 5.42-5.33 (m, 4H), 3.66 (t, 2 h, $J = 6.6$ Hz), 2.80 (m, 2H), 2.07 (m, 4H), 1.59 (m, 2 h), 1.39-1.31 (m, 16H), 1.26 (broad s, 1H), 0.91 (t, 3H, $J = 7.0$ Hz), ^{13}C {^1H} NMR (126 MHz, $CDCl_3$) δ (ppm): 130.20, 130.10, 128.01, 127.93, 63.07, 32.81, 31.52, 29.64, 29.48, 29.39, 29.34, 29.22, 27.20, 25.73, 25.63, 22.55, 14.03. One C is missing. High-resolution mass spectrometry calculated for $C_{18}H_{34}ONa$ $[M+Na]^+$ 289.2501 found 289.2503. Furthermore, triphenylphosphine (1.90 g, 7.3 mmol), carbon tetrabromide (2.16 g, 6.5 mmol), and dichloromethane (DCM) (15 mL) were added in a round bottom flask at 0°C, and the mixture was stirred for 10 minutes. The (9Z, 12Z)-octadecadien-1-ol (965.9 mg, 3.6 mmol) in dichloromethane (10 mL) was transferred on the mixture via cannula at 0°C. A white precipitate was formed. The reaction mixture was warmed up overnight and then was filtered over celite and concentrated under reduced pressure. The product was purified by column chromatography on SiO_2 (petroleum ether/ ethyl acetate (9:1), Rf = 0.90). $m_{pure} = 0.96$ g. Aspect: colorless oil. Yield: 80%. ^1H NMR (500 MHz, $CDCl_3$) δ (ppm): 5.42-5.34 (m, 4H), 3.43 (t, 2 h, $J = 6.9$ Hz), 2.79 (m, 2H), 2.07 (m, 4H), 1.88 (m, 2 h), 1.45 (m, 2 h), 1.39-1.31 (m, 14H), 0.92 (t, 3H, $J = 7.0$ Hz), ^{13}C {^1H} NMR (126 MHz, $CDCl_3$) δ (ppm): 130.20, 130.10, 128.01, 63.07, 32.81, 31.52, 29.64, 29.48, 29.39, 29.34, 29.22, 27.20, 25.73, 25.63, 22.55, 14.03. One C is missing. High-resolution mass spectrometry calculated for $C_{18}H_{32}Br$ $[M-H]^+$ 327.1681 found 327.1682. In a Schlenk flask, diethyl phosphate (0.34 mL, 2.6 mmol) and tetrahydrofuran (2 mL) were introduced. The mixture was cooled to 0°C, and sodium bis(trimethylsilyl)amide (NaHMDS) 2M (1.5 mL, 3.0 mmol) was added. The mixture was stirred at room temperature (20°C–25°C) for half an hour. Then the reaction was cooled to 0°C, and (6Z, 9Z)-18-bromooctadeca-6,9-diene (0.35 g, 1.07 mmol) in tetrahydrofuran (2 mL) was transferred to reaction mixture via cannula. After 30 minutes, the mixture was stirred overnight at 25°C. The reaction medium was concentrated under reduced pressure and purified by column chromatography on SiO_2 (petroleum ether/ethyl acetate (1:4), Rf = 0.50). $m_{pure} = 0.35$ g. Aspect: slightly yellow oil. Yield: 85%. ^1H NMR (500 MHz, CD_2Cl_2) δ (ppm): 5.44-5.34 (m, 4H), 4.12-4.03 (m, 4H), 2.82 (m, 2 h), 2.09 (m, 4H), 1.74-1.68 (m, 2 h), 1.62-1.57 (m, 2 h), 1.39-1.32 (m, 22 h), 0.93 (t, 3H, $J = 7.0$ Hz), ^{13}C {^1H} NMR (126 MHz, CD_2Cl_2) δ (ppm): 130.08, 130.02,

Table 10. Micronucleus Analysis of NKS-5: Short Treatment in the Absence of S9 Mix

Treatment	Concentration in culture medium	Total BN cells scored	Total MNBN cells scored	MNBN cells frequency (%)	Mean frequency (%)
Dimethyl sulfoxide	1% (v/v)	1000	7	0.7	1.025
		1000	10	1.0	
		1000	12	1.2	
		1000	12	1.2	
NKS-5	2.5 mmol/L	1000	11	1.1	0.95
		1000	8	0.8	
	5 mmol/L	1000	13	1.3	1.20
		1000	11	1.1	
	10 mmol/L	1000	9	0.9	0.85
		1000	8	0.8	
Mitomycin C	0.05 μg/mL	1000	106	10.6	10.35
		1000	101	10.1	

BN, binucleate cells; MNBN, micronucleated binucleate cells.

Table 11. Micronucleus Analysis of NKS-3: Short Treatment in the Presence of S9 Mix

Treatment	Concentration in culture medium	Total BN cells scored	Total MNBN cells scored	MNBN cells frequency (%)	Mean frequency (%)
Dimethyl sulfoxide	1% (v/v)	1000	6	0.6	0.60
		1000	6	0.6	
		1000	5	0.5	
		1000	7	0.7	
NKS-3	0.025 mmol/L	1000	7	0.7	0.70
		1000	7	0.7	
	0.05 mmol/L	1000	8	0.8	0.70
		1000	6	0.6	
	0.10 mmol/L	1000	6	0.6	0.50
		1000	4	0.4	
Cyclophosphamide	5 μg/mL	1000	23	2.3	2.70
		1000	31	3.1	

BN, binucleate cells; MNBN, micronucleated binucleate cells.

127.92, 127.87, 61.19 (d, $J = 6.3$ Hz), 31.51, 30.62, 30.49, 29.63, 29.33, 29.24 (d, $J = 6.3$ Hz), 29.05, 27.15 (d, $J = 2.8$ Hz), 26.11, 25.55, 25.00, 22.53, 22.40 (d, $J = 5.3$ Hz), 16.26 (d, $J = 5.3$ Hz), 13.79. ^{31}P NMR (^{1}H) (203 MHz, $CDCl_3$) δ (ppm): +32.05 (s). IR (neat cm-1): ν: 3009, 2926, 2855, 1463, 1392, 1245, 1164, 1097, 1056, 1028, 954, 785, 722. High-resolution mass spectrometry calculated for $C_{22}H_{44}O_3P$ $[M+H]^+$ 387.3023 found 387.3019.

NKS-5 (9Z,12Z)-(3-methyloxetan-3-yl)methyl octadeca-9,12-dienoate, i.e., $C_{23}H_{40}O_3$) was also synthetized from LA by using the following design strategy composed of 3 steps, resulting in the final synthesis:

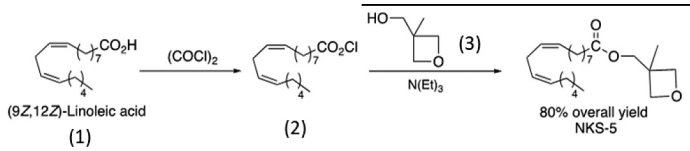

Linoleic acid (1.24 mL, 4.0 mmol) and dichloromethane (8 mL) were introduced under inert atmosphere in a round bottom flask. The mixture was cooled to 0°C, and oxalyl chloride (0.38 mL, 4.4 mmol) was introduced dropwise. Then, the catalytic quantity of dimethylformamide (DMFO) (0.03 mL) was added. The reaction mixture was stirred for 1 hour at 0°C and for 2 hours at room temperature (20°C–25°C). Solvents and oxalyl chloride were removed under reduced pressure, and the product was directly engaged in the following step (aspect: colorless oil with slight precipitate). A solution of 3-methyl-3-oxetane methanol (0.52 mL, 5.2 mmol), triethylamine (0.73 mL, 5.2 mmol) in tetrahydrofuran (20 mL) was prepared in a round bottom flask under inert atmosphere. The mixture was cooled to 0°C, and freshly prepared linoleoyl chloride (1.16 g, 4.0 mmol) in tetrahydrofuran (20 mL) was added via cannula. After stirring for 1 hour at room temperature, the mixture was worked up by addition of distilled water

Table 12. Micronucleus Analysis of NKS-5: Short Treatment in the Presence of S9 Mix

Treatment	Concentration in culture medium	Total BN cells scored	Total MNBN cells scored	MNBN cells frequency (%)	Mean frequency (%)
Dimethyl sulfoxide	1% (v/v)	1000	9	0.9	0.975
		1000	11	1.1	
		1000	8	0.8	
		1000	11	1.1	
NKS-5	2.5 mmol/L	1000	10	1.0	1.05
		1000	11	1.1	
	5 mmol/L	1000	9	0.9	0.90
		1000	9	0.9	
	10 mmol/L	1000	9	0.9	0.85
		1000	8	0.8	
Cyclophosphamide	10 μg/mL	1000	82	8.2	8.05
		1000	79	7.9	

BN, binucleate cells; MNBN, micronucleated binucleate cells.

Table 13. Micronucleus Analysis of NKS-3: Extended Treatment in the Absence of S9 Mix

Treatment	Concentration in culture medium	Total BN cells scored	Total MNBN cells scored	MNBN cells frequency (%)	Mean frequency (%)
Dimethyl sulfoxide	1% (v/v)	1000	10	1.0	0.90
		1000	8	0.8	
		1000	10	1.0	
		1000	8	0.8	
NKS-3	0.0065 mmol/L	1000	8	0.8	0.70
		1000	6	0.6	
	0.010 mmol/L	1000	8	0.8	0.85
		1000	9	0.9	
	0.020 mmol/L	1000	9	0.9	0.75
		1000	6	0.6	
Vinblastine	0.0025 μg/mL	1000	115	11.5	11.9
		1000	123	12.3	

BN, binucleate cells; MNBN, micronucleated binucleate cells.

(6 mL). The product was extracted with ethyl acetate (3 × 15 mL), dried over $MgSO_4$, and purified by column chromatography on SiO_2 (petroleum ether/ ethyl acetate (5:1), Rf = 0.70). m_{pure}= 0.85 g. Aspect: colorless oil. Yield: 80%. ^{1}H NMR (500 MHz, $CDCl_3$) δ (ppm): 5.39-5.36 (m, 4H), 4.54 (d, 2 h, J = 6.0 Hz), 4.40 (d,2 h, J = 6.0 Hz), 4.18 (s, 2 h), 2.79 (t, 2 h, J = 6.9 Hz), 2.37 (t, 2 h, J = 7.5 Hz), 2.07 (q, 4H, J = 6.8 Hz), 1.66 (m, 2 H, J = 7.2 Hz), 1.38-1.31 (m, 17H), 0.91 (t, 3H, J = 6.9 Hz). ^{13}C {^{1}H} NMR (126 MHz, $CDCl_3$) δ (ppm): 174.00, 130.36, 130.15, 128.22, 128.05, 79.74, 68.60, 39.26, 34.36, 31.67, 29.73, 29.48, 29.29, 29.26, 29.24, 27.34, 27.32, 25.78, 25.12, 22.70, 21.34, 14.19. One C is missing. IR (neat cm-1): ν: 3010 (small), 2928 (broad), 2857 (broad), 1739, 1460, 1378, 1351, 1240, 1163 (broad), 1099, 984, 942, 834, 723 (broad). High-resolution mass spectrometry calculated for $C_{23}H_{41}O_3$ $[M+H]^+$ 365.3050 found 365.3043. All reactions, unless stated otherwise, were carried out using standard Schlenk techniques under an inert atmosphere. Dichloromethane, toluene, pentane, tetrahydrofuran, and diethylether were dried using a MBRAUN SPS 800. Commercially available diethylphosphite, oxalyl choride, sodium bis(trimethylsilyl) amide 2M, linoleic acid (99% purity and technical grade), and 3-methyl-3-oxetane methanol were used without purification. Thin layer chromatography was performed on silica chromagel (60 μm F_{254}) and exposed by UV, potassium permanganate, or iodine treatment. Flash chromatography was carried out with the indicated solvents using silica gel 60 (60AAC, 35-70 μm). The ^{1}H (and ^{1}H decoupled), ^{13}C, and ^{31}P NMR spectra were recorded on 600, 500, 400, or 300 MHz spectrometers at ambient temperature using tetramethylsilane as internal reference for ^{1}H and ^{13}C spectra and phosphoric acid (85%) as external reference for ^{31}P NMR. Data were reported as s = singlet, d = doublet, t = triplet, q = quartet, m = multiplet, br.s = broad signal, coupling constant(s) in Hertz, integration. Infrared spectra were recorded on FT-IR instrument, and the data are given in cm^1. Melting points were measured on a Kofler melting points apparatus and are uncorrected. Optical rotation values were determined at 20°C on a polarimeter at 589 nm (sodium lamp). The mass spectra and accurate mass measurements were performed under (ESI) conditions with a micro Q-TOF detector or Orbitrap detector or in the MALDI/ TOF reflection mode using dithranol as a matrix.

Table 14. Micronucleus Analysis of NKS-5: Extended Treatment in the Absence of S9 Mix

Treatment	Concentration in culture medium	Total BN cells scored	Total MNBN cells scored	MNBN cells frequency (%)	Mean frequency (%)
Dimethyl sulfoxide	1% (v/v)	1000	11	1.1	1.175
		1000	13	1.3	
		1000	11	1.1	
		1000	12	1.2	
NKS-3	2.5 mmol/L	1000	9	0.9	0.80
		1000	7	0.7	
	5 mmol/L	1000	8	0.8	0.85
		1000	9	0.9	
	10 mmol/L	1000	10	1.0	0.95
		1000	9	0.9	
Vinblastine	0.025 μg/mL	1000	46	4.6	4.35
		1000	41	4.1	

BN, binucleate cells; MNBN, micronucleated binucleate cells.

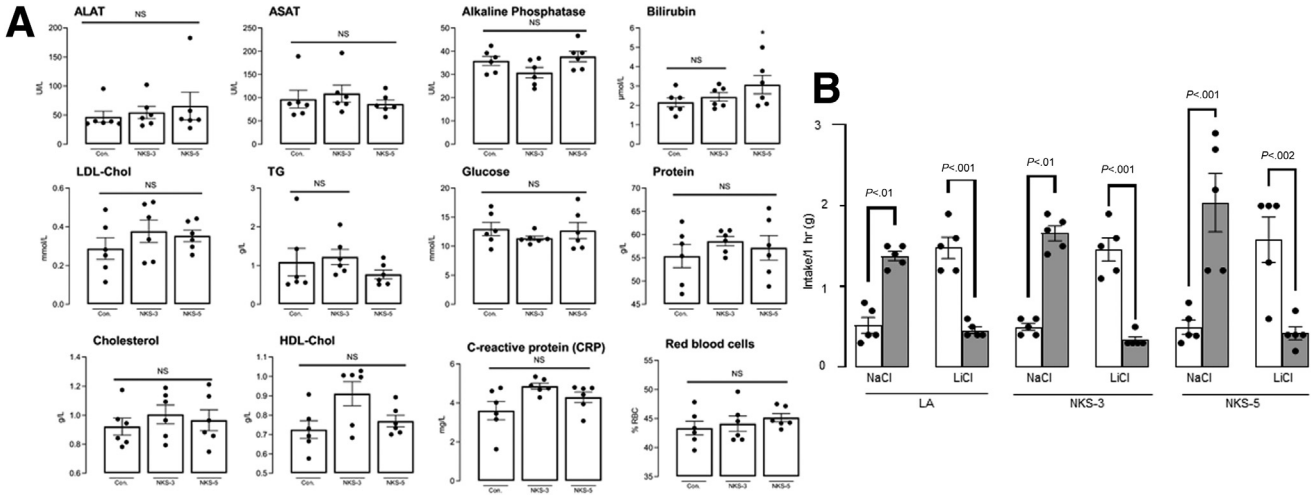

Figure 12. FTA exert no toxicological effects and malaise in conditioned taste aversion (CTA). In (*A*), female pathogen-free Wistar rats (8- to 12-week-old) were quarantined for 7 days. After quarantine, rats were randomized and assigned to 3 groups (5 rats/group) where group 1 (control) received the vehicle (0.3% xanthan gum), group 2 received NKS-3, and group 3 received NKS-5. After an overnight fast, rats were weighed (180–200 g) and dosed orally by gavage with a single limit dose of 2000 mg/kg body weight of NKS-3 or NKS-5. This dosage was selected on the basis of a preliminary study performed with single animal in which no evidence of toxicity was observed at oral dosages of 5000 mg/kg body weight. At the end of the observation period (2 weeks), all rats were weighed after anesthesia by isoflurane inhalation, and cardiac blood samples were collected for biochemical analysis. Data are mean ± SEM (n = 6). No significant difference was observed between the groups (compared with control), analyzed by means of repeated measure two-way analysis of variance, followed by Tukey multiple comparison test. In (*B*), CTA, performed by pairing a conditioned stimulus, ie, LA or FTA (NKS-3 or NKS-5) with a digestive pain caused by intraperitoneal injection of LiCl (150 mmol/L, 16.5 μL/g of body weight), was assessed by using 1 hour 2-bottle paradigm where one bottle contained xanthan gum (0.3%, blank histograms), and the second bottle contained LA (2%) or NKS-3 (50 μmol/L) or NKS-5 (75 μmolk/L). The control unconditioned animals received intraperitoneal NaCl at the same concentration. Data are means ± SEM (n = 5). Unpaired two-tailed Student *t* test was used.

Modeling the Full-Length Structure of CD36

The crystal structure of CD36 (PDB code 5LGD:A) covers only the residues 35-434, which constitute the extracellular domain of this membrane protein. According to UniProt annotation of CD36 (UniProtKB – P16671), the regions 8-29 and 440-461 are transmembrane helices, which are likely to form an antiparallel bundle in the membrane, considering the spatial proximity of the residues 35 and 434 in the crystal structure. Unfortunately, the transmembrane helices, the missed linkers to extracellular domain, and the intracellular termini have no homologs among the proteins with known structure. Thus, automated homology modeling for this protein does not produce any useful results. C-I-TASSER,[47] I-TASSER,[47] and GalaxyTBM[48] servers predict either disordered coils in place of transmembrane helices or highly distorted helices with wrong orientation. Such widely used servers as ModWeb and SwissModel failed to produce any structure for transmembrane helices at all because of the absence of any homologs. The MEMPACK server failed to produce any confident prediction of the arrangement of transmembrane helices, despite the fact that they were identified correctly in the primary sequence. The MemBrain predicted completely wrong protein topology with multiple membrane spanning helices instead of the large globular extracellular domain. The only tool that produced meaningful results for the membrane region of CD36 was PREDDIMER server.[49] With the regions 8-29 and 440-461 considered as antiparallel transmembrane helices according to UniProt annotaion of CD36, it generated 5 most probable packings of helices with different tilt and contacting residues.

Thus, we used crystal structure of CD36 (PDB code 5LGD:A) as a template for the residues 35-434 and the

Table 15. Weight (in g) of Different Organs in Median Lethal Dose Studies

Organs	Control	NKS-3	NKS-5
Liver	8.19 ± 0.61	8.12 ± 0.188	8.03 ± 0.136
Spleen	0.91 ± 0.03	0.96 ± 0.12	0.90 ± 0.062
Kidneys	1.87 ± 0.06	1.82 ± 0.193	1.84 ± 0.112

NOTE. The weight of different organs was taken just after the death of rats, administered or not with NKS-3 or NKS-5. Data are means ± SEM (n = 5).

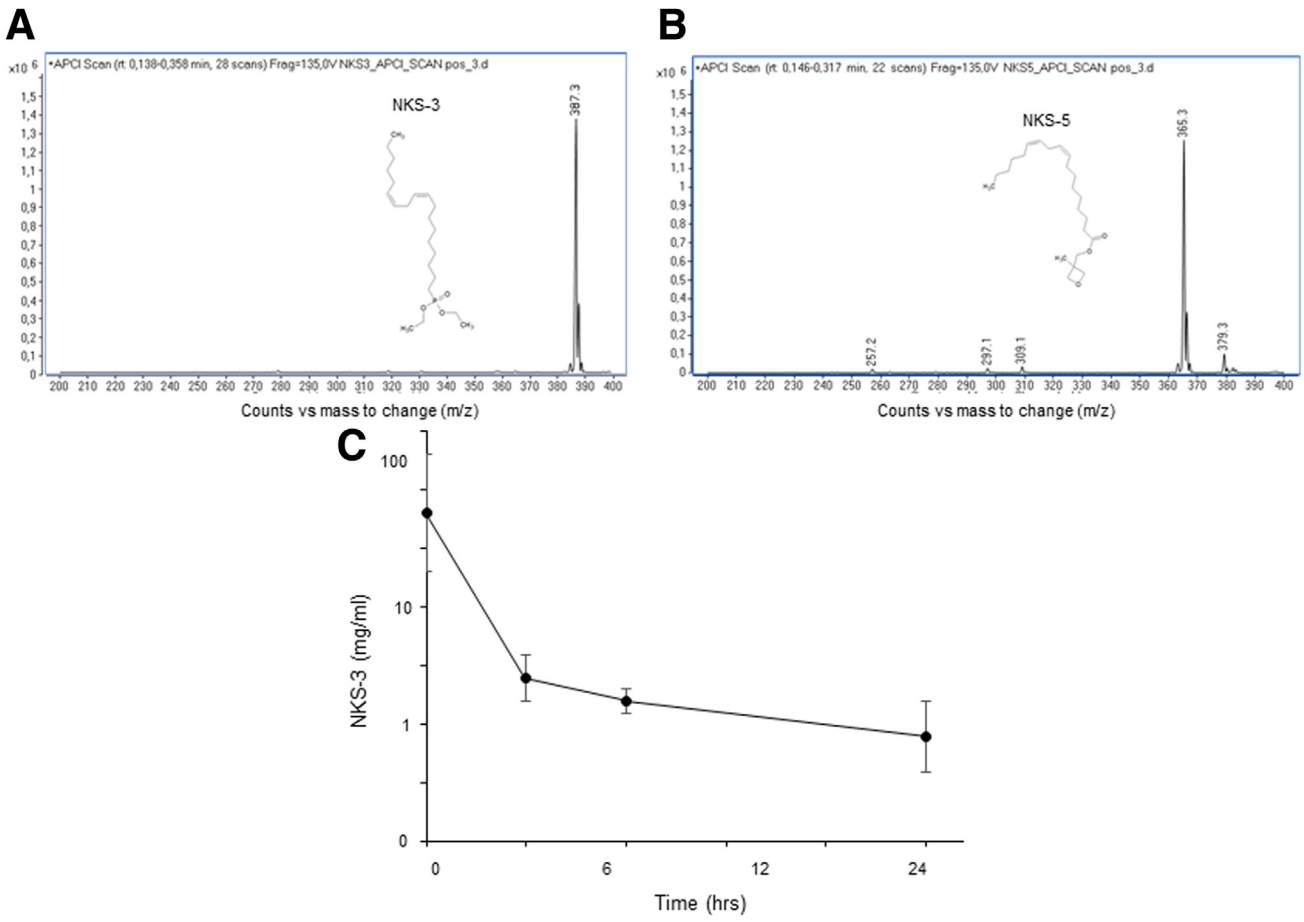

Figure 13. FTA detection and pharmacokinetic NCA analysis. Detection of NKS-3 and NKS-5 by liquid chromatography-mass spectrometry (LC-MS). (*A* and *B)* Atmospheric pressure chemical ionization (APCI) positive SCAN profiles of NKS-3 and NKS-5, respectively. (*C)* Pharmacokinetics representing non-compartmental analysis (NCA). Mice were injected intravenously with NSK-3, 5 mice per group. A total of 100 μL of blood sample was drawn at the indicated times. NSK-3 concentrations were assessed by LC-MS. Values are represented as mean ± SEM *(*n = 5). Mean pharmacokinetic parameters for each condition were compared to sort out any differences.

structures predicted by PREDDIMER as templates for the residues 8-29 and 440-461. The sequence alignment of templates and the full-length sequence of CD36 were generated using MultiSeq plugin of VMD. The Modeller 9.2[50] was used to generate missed parts of the structure. We used the secondary structure prediction from C-I-TASSER server[47] to impose secondary structure restraints for the linkers between extracellular domain and the transmembrane helices. Particularly, the regions 7-40 and 424-465 were restrained as continuous alpha-helices, whereas intracellular N- and C-terminals were considered as coils. The automodel protocol of Modeller was used with "slow"

Table 16. Pharmacokinetic Parameters for NKS-3

Study	Unit	Values (means ± SEM)
C_{max}	mg/kg/L	46.73 ± 15.25
T_{max}	min	5[a]
AUC_{last}	mg/kg/Lxh	59.94 ± 12.09
Clearance	L/h	0.169 ± 0.028
Vd_{ss}	L/kg	1.23 ± 0.279

NOTE. Animals were intravenously injected with NKS-3 at the dose of 10 mg/kg body weight. The parameters (C_{max}, T_{max}, $AUC_{0-6\ h}$, Vd_{SS}) were determined using a standard non-compartmental approach (NCA). Five mice per group. All of the NCA calculations were performed with Kinetica Software (Thermo Scientific, Philadelphia, PA).
AUC, area under the plasma concentration-time curve; C_{max}, maximum plasma concentration; T_{max}, the time to reach C_{max}; Vd_{SS}, volume of distribution (Vd) during steady-state (SS).
[a]Median.

Table 17. Interindividual Variabilities Associated to the Population Pharmacokinetic Parameters for NSK-3

	Estimation mean	Interindividual variability (coefficient of variation, %)
Clearance (*L*/*h*)	0.202	44.1
Volume of central compartment (*L*)	0.0634	NC
Intercompartmental clearance (*L*/*h*)	0.739	66.7
Volume of peripheral compartment (*L*)	2.24	24.8
Proportional residual error (%)	1.89	—

level of optimization. Five models were generated for each variant of the transmembrane helices packing, which results in 25 models. The models were ranked by their DOPE scores, and 2 best models were selected. The structures were examined visually, and the model where extracellular domain is more perpendicular to the presumed membrane plane was chosen. At the absence of any experimental data about preferable orientation of the extracellular domain in respect to the membrane, such choice eliminates possible biased interactions between this domain and the lipid head groups as much as possible.

To keep all glycosylated residues and to eliminate any distortion of the extracellular domain, which may have happened during structure optimization in Modeller, we aligned produced model to the crystal structure of CD36 by the residues 57-387 and substituted this segment explicitly by the crystal structure.

Modeling the Full-Length Structure of GPR120

There is no crystal structure of GPR120 protein available to date. I-TASSER[47] server with default parameters was used to build the homology model of this protein. The best scored model was used for subsequent simulations. The model contains long extracellular loops that lack secondary structure and share no significant sequence similarity to available templates with known structure. Although the quality of modeling of these loops remains questionable, they are located far from predicted binding site of the protein. Considering general structural rigidity of rhodopsin-like seven-bundle family of proteins, which includes GPR120, it is unlikely that these loops will influence the conformation of the binding site. Thus, no additional model refining was performed.

Binding Site Identification

The binding site of CD36 protein is known because 2 fatty acid molecules are present in the crystal structure 5LGD:A. The residues of the binding site were identified as located within 0.5 nm from any of these fatty acids. In contrast, the binding site of GPR120 is not known. We used the binding site predictions provided by I-TASSER and C-I-TASSER servers based on multiple structural templates. We filtered out those templates, which predict the binding site for cholesterol located on the outer membrane-faced surface of the protein. Remained templates 4MQS:A, 4EA3:B, and 4RNB:A predict the binding site location inside the protein helical bundle.

Molecular Dynamics Simulations

The CD36 protein was inserted into POPC lipid membrane using CHARMM GUI membrane builder tool.[50] The orientation of the protein followed orientation of the transmembrane helices predicted by PREDDIMER. In addition to 9 glycosylated residues present in the crystal structure, the residue 163 was glycosylated with N-acetyl-D-glucosamine, and the residues 3, 7, 464 and 466 were palmitoylated as suggested by annotation in the UniProt database. Resulting system contained 284 POPC lipids, ~40,000 water molecules. One hundred eighteen Na^+ and 121 Cl^- ions correspond to ionic strength of ~0.15 mol/L and counterbalance the net charge of protein. All palmitoylated residues appeared in the intracellular leaflet of the membrane, which is in agreement with experimental data.[51] The system was equilibrated in several steps. First, the membrane and solution were equilibrated for 50 ns with all protein atoms restrained. Then, the system was equilibrated for 100 ns with the protein backbone restrained. Finally, all restrains were removed, and production run of 200 ns was performed.

GPR120 was inserted into the membrane using the same technique. The residue ASN 20 was glycosylated with N-acetyl-D-glucosamine according to annotation in the UniProt database. Resulting system contained 218 POPC lipids, ~22,000 water molecules, 45 Na^+ ions, and 58 Cl^- ions. The membrane and solution were equilibrated for 25 ns with all protein atoms restrained. Then, the system was equilibrated for 50 ns with the protein backbone restrained. Finally, all restrains were removed, and production run of 100 ns was performed.

All molecular dynamic simulations were performed in Gromacs versions 2019.2 in NPT ensemble at the pressure of 1 atm maintained by Parrinello-Rahman barostat with semi-isotropic pressure coupling. The Verlet cutoff scheme was used. Force-switch cutoff of the Van der Waals interactions was used in the region between 1.0 and 1.2 nm. Long range electrostatics was computed with the PME method, with the cutoff of explicit short-range electrostatic interactions at 1.2 nm. Velocity rescale thermostat was used at the temperature of 310K. CHARMM36 force field was used for all components of the system. An integration step of 2 fs was used in all simulations, with the bonds to hydrogen atoms converted to rigid constraints. Analysis was performed by the custom scripts based on Pteros molecular modeling library.[52] To investigate this in more detail, we computed probabilities P_i of particular residue i to be in contact with the ligand:

$$P_i = \frac{\sum_{j=1}^{N} \delta_{ij}}{N}$$

where i is the residue index, j is the index of docking simulation, N is the number of docking simulations, δ_{ij} is a coefficient that is 1 if i-th residue is in contact with the ligand in the j-the docking simulation and 0 otherwise. The residue was considered to be in contact with the ligand if any of its

heavy atoms is located within 0.35 nm from any atom of the ligand.

To account for protein conformational flexibility multiple conformations from molecular dynamic trajectories were extracted and used in docking simulations. Last 50 ns of molecular dynamic trajectories were used to extract 834 equally spaced frames. For each frame, the docking of 3 ligands LA, NKS-3, and NKS-5 was performed. The docking space was centered in the center of mass of the protein binding site and had dimensions 2 × 2 × 2 nm. Quick Vina 2 docking software was used with default scoring function. The best docking pose was kept in each simulation. The methodology and scripts for ensemble docking have been used in our previous work.[47] No side chains were treated as flexible because possible flexibility was already accounted for by means of molecular dynamic simulations.

NKS-3 and NKS-5 Analyses by Liquid Chromatography-Mass Spectrometry

NKS-3 and NKS-5 stock solutions (1 mg/mL) and working solutions (1 ng/μL) were prepared in methanol and stored at −20°C. NKS-3 calibration standards were realized with 10 μL of a pool of human plasma containing NKS-5 (100 ng) used as internal standard and increasing amounts of NKS-3 (0–128 ng). NKS-5 calibrations were prepared in the same way, using NKS-3 (100 ng) as internal standard and NKS-5 (0–128 ng) as external standard. Plasma samples (10 μL) were spiked to the relative internal standard (100 ng). Ice-cold methanol (up to 500 μL) was mixed with plasma and calibration samples. Each tube was then stored at −20°C for 1 hour and further centrifuged for 10 minutes at 4°C × 20,000*g*. Supernatants were collected and then evaporated to dryness under vacuum. Samples and calibration standards were finally dissolved in methanol (50 μL) and briefly centrifuged for 2 minutes at 4°C × 20,000*g*. Supernatants were transferred into injection vials, and 3 μL was injected into a 1260 LC system coupled to a 6460-QqQ MS/MS system equipped with an APCI source (Agilent Technologies). Separation was achieved on a SBC18 2.1x50 mm, 1.8 μm column (Agilent Technologies) at a flow rate of 0.250 mL/min, 40°C, with a linear gradient of (solvent A) water/methanol 60/40 (v/v) containing ammonium acetate (10 mmol/L), acetic acid (1 mmol/L), and solvent B, ie, propanol-2/methanol 90:10 (v/v) containing ammonium acetate (10 mmol/L) and acetic acid (1 mmol/L), as follows: 55% B up to 100% B in 5 minutes and then maintained at 100% B for 1 minute. Acquisition was performed in positive Single Reaction Monitoring (SRM) mode (gas temperature 325°C, APCI heater 350°C, gas flow rate 4 L/min, 20 psi, capillary voltage 4500 V, APCI needle 6 V). Transitions used were NKS-3 387.3 → 151 (frag 108V, CE 22V), NKS-5 365.4 → 67.1 (frag 108V, CE 26V). NKS-3 calibration curve was calculated using NKS-5 as internal standard. NKS-5 calibration curve was calculated using NKS-3 as internal standard. Results were expressed as μg per milliliter of plasma.

Gut Microbiota Analyses

At the time of death, the fecal samples were taken from the intestine (colon). We did not collect the fecal samples from the cages because the room temperature and aerobic environment might have influenced the bacterial population. The fecal samples were immediately stored at −80°C until their analyses. The microbes present in the samples were determined using next-generation high-throughput sequencing of variable regions of the 16S rRNA bacterial gene. Polymerase chain reaction amplification was performed using 16S universal primers targeting the V3-V4 region of the bacterial 16S ribosomal gene (Vaiomer universal 16S primers). The joint pair length was set to encompass 467 base pairs (2 × 300 paired-end MiSeq kit V3). For each sample, a sequencing library was generated by addition of sequencing adapters. The targeted metagenomic sequences from microbiota were analyzed using the bioinformatics pipeline established by Vaiomer from the FROGS guidelines.

Genotoxic, Mutagenic, and Endocrine Perturbator Studies

The hepatocyte HepG2 cell line was used for assessing genotoxicity.[53] The positive control compounds (mitomycin C, vinblastine, and cyclophosphamide) induced significant increases in the number of binucleate cells containing micronuclei, demonstrating the efficacy of S9 mix and the sensitivity of the test system.[54] The mutagenic activity was performed in the bacterial reverse mutation test using *S typhimurium* tester strains TA98, TA100, TA1535, and TA1537 and *E coli* tester strain WP2*uvrA* (pKM101) in the presence and absence of phenobarbital/5,6-benzoflavone-induced rat liver S9.[55] As regards endocrine disrupter properties, agonist/antagonist activity directed against human estrogen receptor alpha (hERα) and/or human androgen receptor (hAR) were assessed. Hence, reporter gene assays based on stably transfected cell lines were used to screen potential agonist or antagonist activity.

Toxicological and Conditioned Taste Aversion Assays

For the determination of toxicity/median lethal dose as per OECD guidelines 425 (OECD, 2008), we used pathogen-free female Wistar rats, procured from Janvier Elevage (France). The rats were quarantined for 7 days and evaluated for weight gain and any gross signs of disease or injury. After quarantine, rats were randomized and assigned to 3 groups (5 rats/group). Group 1 (control) received orally the vehicle (xanthan gum, 0.3 %, w/v), group 2 received NKS-3, and group 3 received NKS-5 orally. After an overnight fast, rats were weighed (180–200 g) and dosed orally by gavage with a single limit dose of 2000 mg/kg body weight of NKS-3 and NKS-5. This dosage was selected on the basis of a preliminary study performed with single animal/group in which no evidence of toxicity was observed at oral dosages of 5000 mg/kg. NKS-3 and NKS-5 were administered by gavage at a volume of 2.5 ml/kg, which was based on the individual animal body weights obtained on the day of gavage. NKS-3 and NKS-5 were prepared in 0.3 % xanthan gum (w/v) on the day of experiment.

The animals were carefully observed twice daily (AM and PM) for mortality and morbidity until day 15. Other general criteria were as follows: evaluation of skin and fur, eyes and mucous membranes, respiratory, central nervous system effects (tremors and convulsions), autonomic effects (eg, salivation), gait and posture, and changes in the level of motor activity. At the end of the test, animals were weighed and killed after anesthesia by isoflurane inhalation. The cardiac blood samples were collected. The necropsy included a macroscopic examination of the external surface of the body, all orifices, the cranial cavity, the brain, and the thoracic, abdominal, and pelvic cavities and viscera. Samples of the following tissues and organs were collected from all animals at necropsy and fixed in neutral phosphate-buffered 4% formaldehyde solution: jejunum, colon, kidneys, liver, spleen, and adipose tissues.

The CTA assays were performed as described previously.[56] The adult male C57BL/J6 mice, weighing from 21 to 24 g and already acclimatized to the animal facility, were trained to drink water (containing 0.3% xanthan gum) for 1 hour between 10:00 AM and 11:00 AM for 3 days. To avoid dehydration, the mice were also allowed to drink water every day between 3:00 PM and 3:30 PM. On day 4, the animals were divided into 3 groups that received the following solutions in 0.3% xanthan gum: group 1 received 2% LA, group 2 received NKS-3 (5 mmol/L), and group 3 received NKS-5 (5 mmol/L) from 10:00 AM to 11:00 AM and then were immediately injected intraperitoneally with 150 mmol/L LiCl (16.5 μL/g body weight) or 150 mmol/L NaCl solutions (16.5 μL/g body weight, controls). On day 5, the mice were subjected to 2-bottle paradigm where one contained water (0.3% xanthan gum), and the second contained one of the following: LA (0.2%), NKS-3 (50 μmol/L), or NKS-5 (75 μmol/L). The intake (in g) was measured by weighing the bottles before and after 1 hour of test condition.

Pharmacokinetic Parameters

NSK-3 and NSK-5 pharmacokinetics data were analyzed via a non-compartmental approach (Kinetica; Thermo Scientific, Philadelphia, PA) to determine the major pharmacokinetic parameters (ie, C_{max}, T_{max}, AUC_{last}, $T_{1/2}$, clearance, and V_{ss}). Parameters were derived for each animal and then summarized as means or medians (for time). A second approach, called population pharmacokinetic, was applied to propose an optimal limited sampling strategy approach that is based on non-linear mixed effect modeling (Monolix; Lixoft, Paris). The aim is to propose a model that, via a compartmental approach, underlies the entire time course of the concentrations versus time by differential equations.

Isolation of TBC From Mouse and Human Fungiform Papillae

The fasted mice were killed, and lingual fungiform papillae were isolated according to previously published procedure.[57] In brief, a mixture of enzymes (elastase and dispase mixture, 2 mg/mL each, in Tyrode buffer: 120 mmol/L, NaCl; 5 mmol/L, KCl; 10 mmol/L, HEPES; 1 mmol/L, $CaCl_2$; 1 mmol/L, $MgCl_2$; 10 mmol/L, glucose; 10 mmol/L, Na-pyruvate, pH 7.4) was used to isolate the lingual epithelium. The peeled epithelium was further treated with an enzyme mixture (2 mmol/L EDTA, 1.2 mg/mL elastase, 0.6 mg/mL type I-collagenase), and 0.6 mg/mL trypsin inhibitor to dissociate TBC. The supernatant containing released cells was used to isolate TBC by centrifugation at 20,000g $\times$ 10 minutes.

Human fungiform papillae were isolated from the donors that were admitted to the Stomatology Department of the Hospital (Dijon). Human fungiform papillae were picked off by using scissors under local anesthesia and subjected to enzymatic digestion that contained elastase and dispase mixture (as used for mice TBC).[58] The isolated cells were cultured for 24 hours in a mixture of Iscove's modified Dulbecco medium and MCDB 153, supplemented with 10% fetal bovine serum and antibiotics. Furthermore, the cells were transfected for 8 hours with h-tert lentivirus, and after 15 days of culture, some clones were picked off and expanded until their characterization.

Measurement of Ca^{2+} Signaling

The TBC were washed with a buffer (3.5 mmol/L, KH_2PO_4; 17.02 mmol/L, Na_2HPO_4; 136 mmol/L, NaCl, pH 7.4) and incubated with Fura-2/AM (1 μmol/L) for 60 minutes at 37°C in loading buffer that contained the following: 110 mmol/L, NaCl; 5.4 mmol/L, KCl; 25 mmol/L, $NaHCO_3$; 0.8 mmol/L, $MgCl_2$; 0.4 mmol/L, KH_2PO_4; 20 mmol/L, HEPES-Na; 0.33 mmol/L, Na_2HPO_4; 1.2 mmol/L, $CaCl_2$, pH 7.4. Later, the cells (2 $\times$ 10^6/mL) were washed 3 times (600g $\times$ 10 minutes) and remained suspended in the identical buffer. The changes in free intracellular Ca^{2+} concentrations, $[Ca^{2+}]i$, were monitored under the Nikon microscope (TiU) by using S-fluor 40$\times$ oil immersion objective. The planes were taken at Z intervals of 0.3 μm, and NIS-Elements software was used to deconvolve the images. The microscope was equipped with EM-CCD (Lucas) camera for real-time recording of 16-bit digital images. The changes in $[Ca^{2+}]i$ were expressed as F_{340}/F_{380} ratio.

Lingual Application of FTA and Pancreato-bile Secretions

To assess the effect of oral deposition of FTM and other agents on PB secretions and the release of gut peptides, mice were fasted for a period of 12 hours and then used for the experiments.[26] The esophagus was ligated to avoid any ingestion. A catheter was placed, closed to the duodenum, to collect pancreatic/bile secretions. At first, we determined basal secretions, and then the fatty acid or FTA were gently placed, with the help of a pipette, onto the tongue in such a way that the application covered tongue epithelium containing fungiform papillae. The secretion was collected as mentioned in the legends. The protein contents of the secretions were determined as per standard lab method. In the similar set of experiments, we bled the animals and collected blood from the tail to determine the release of gut peptides for a time period mentioned in the legends.

CT Nerve Recordings

For measurements of CT activity, adult male C57BL/J6 mice ranging in weight from 21 to 24 g were anesthetized

with intraperitoneal administration of ketamine (30 mg/kg) followed by urethane (1.2 g/kg), with further doses as necessary. The animal's corneal reflex and pedal reflex were used to monitor the depth of surgical anesthesia. A tracheotomy was performed to prevent suffocation. To access the CT nerve, we secured the tracheotomized mouse in a non-traumatic head holder and used the mandibular approach to expose the left CT nerve.[59] Then, it was dissected free from the surrounding tissues and cut at the point of its entry into the bulla. The CT nerve was placed on the Ag–AgCl electrode (positive polarity). The entire cavity was then covered with mineral oil to isolate the nerve signal from ground and nerve integrity. An indifferent electrode (negative polarity) was attached to the skin overlying the cranium with an alligator clip and served as a reference. Throughout the surgery and nerve recordings, body temperatures were maintained at 37° with a thermal pad.

Signals were first amplified and passed through a band-pass filter (300–3000 Hz) by an AC differential amplifier (DAM 80; WPI, USA). Thereafter, signals were digitized (sampling rate: 1000 samples/s), integrated with a time constant of 1.0 s, and then sorted for on-line data collection using a laboratory interface and software (PowerLab 4/30; ADInstruments Pvt Ltd, Australia). All electrical activity was also displayed on an oscilloscope (Hitachi, Japan). The unit activities were also assessed simultaneously by the use of an audio analyzer instrument (Fredrick Haer, USA). All taste solutions were mixed daily from reagent grade chemicals (Sigma-Aldrich and VWR) and presented at room temperature. Stimuli consisted of NKS-3, NKS-5, LA, and OA at 1, 2, and 4 mmol/L concentrations. In addition, 0.1 mol/L NH_4Cl mixed in distilled water was applied before and after each concentration series, with a given taste stimulus serving as a reference stimulus. The anterior half of the mouse tongue was enclosed in a flow chamber. Solutions were delivered into the flow chamber through input tubes by gravity flow and flowed over the tongue for a controlled period (0.1 ml/s). For data analysis, the magnitude of the integrated neural activities was measured and averaged at 6 different time points for 1 minute after stimulus (at 5, 15, 25, 35, 45, and 55 seconds). Finally, data were normalized to the response magnitude of 0.1 mol/L NH_4Cl.

Diet-Induced Obesity

The C57BL/6J male mice were randomly grouped and fed with either of the following diets: STD or HFD (Table 1). The diets were given for 26 weeks. After a period of 10 weeks with either of the diets (STD or HFD), the animals were divided into 3 groups: control group, NKS-3 (50 μmol/L in 0.3% xanthan gum, w/v) or NKS-5 (75 μmol/L in 0.3%, w/v) in the water bottles until the completion of week 26. The control group received water-containing vehicle (0.3% xanthan gum, w/v). Every 2 days, the food and water intake were measured. At the end of the experiment, mice were fasted overnight, blood samples were collected by cardiac puncture into heparinized tubes, and then killed by cervical dislocation without anesthesia to avoid any further stress. Liver and adipose tissues were dissected, weighed, and then rapidly snap-frozen in liquid nitrogen and stored at –80°C. The plasma was immediately separated and stored at –80°C until used for further analysis.

Two-Bottle Preference and Licking Tests

Two-bottle preference test was performed as described previously.[1] The mice were placed individually in cages. Mice were deprived of water for 6 hours before the experiment. They were first subjects to routine conditioning preference while they are subjected to 2 bottles: one containing water and another containing 4% sucrose (w/v). Once we also interexchanged the placement of bottles to avoid any preference for a particular bottle, ie, habituation. They were subjected to choose between a control solution (0.3% xanthan gum, w/v) and a test solution containing one of the agents: NKS-3, NKS-5, 0.2% canola oil, or LA (7.4 mmol/L) as mentioned in the legends, over a period of 12 hours. The intake was determined by weighing the drinking bottles at the end of experiment. For the licking tests, the mice fasted for 6 hours were exposed to water bottles in a contact lickometer (Med Associates, St Albans, VT).[60] After a training period, which was required to learn the procedure, mice were randomly subjected to a bottle that contained one of the solutions: vehicle control (0.3% xanthan gum, w/v), NKS-3 (50 μmol/L in vehicle), NKS-5 (75 μmol/L in vehicle), or LA (7.4 μmol/L in vehicle) for 1 or 5 minutes.

Real-Time Quantitative Polymerase Chain Reaction

Total RNA was extracted by using TRIzol according to the manufacturer's recommendations (Invitrogen, Cergy-Pontoise, France). For the extraction of total RNA from adipose tissue, the RNeasy Mini Kit (Qiagen) was used. The RNA was quantified by determining its UV absorbance at 260 nm. cDNA was generated simultaneously for all samples by using the High-Capacity cDNA Reverse Transcription Kit according to the manufacturer's recommendations. cDNA was amplified using a StepONePlus (Life Technologies, Saint-Aubin, France) device with the use of SYBR green PCR Master Mix (Life Technologies, Saint-Aubin, France). Quantitative real-time polymerase chain reaction was carried out using the following protocol: holding stage 1 cycle at 95°C for 10 minutes and 45 cycles of cycling stage at 95°C for 15 seconds, 60°C for 1 minute, and multi-curve stage at 95°C for 15 seconds and 60°C for 1 minute. The relative mRNA expression was calculated by the cycle threshold method ($\Delta\Delta$Ct). The samples were run in duplicate, and mRNA expression was normalized to β-actin or GAPDH as housekeeping genes. The calculations were performed by a comparative method (2.0-Ct). Primers used for quantitative polymerase chain reaction analysis are shown in Table 18.

Intraperitoneal Glucose Tolerance Test

To evaluate the effects of FTA on insulin sensitivity, IPGTT was performed on mice after 26 weeks of a feeding period. After 12 hours of food deprivation, a glucose solution (20% w/v) was administered intraperitoneally at 2 g/kg body weight.

Table 18. Primer Sequences for Real-time Quantitative Polymerase Chain Reaction

Genes	Forward primers	Reverse primers
β-actin	5′-CTGGTCGTACCACAGGCATT-3′	5′-CTCTTTGATGTCACGCACGA-3′
GAPDH	5′-CTACCCCCAATGTGTCCGTCG-3′	5′-TGAGGTCCACCACCCTGTTGC-3′
CD36	5′-CCGAACACAGCGTAGATAGAC-3′	5′-GGCCAAGCTATTGCGACATG-3′
FAS	5′-GGCTCTATGGATTACCCAAGC-3′	5′-CCAGTGTTCGTTCCTCGGA-3′
SREBP1	5′ -CCCACCTCAAACCTGGATCT-3′	5′ -AAGCAGCAAGATGTCCTCCT-3′
SCD1	5′-CTACAAGCCTGGCCTCCTGC-3	5′-GGACCCCAGGGAAACCAGGA-3′
PPAR-γ	5′- CCTGCGGAACCCTTTGGTGACTT-3′	5′-TTCACGTTCAGCAAGCCTGGGC-3′
IL1β	5′-CACAGCAGCACATCAACAAG-3′	5′-GTGCTCATGTCCTCATCCTG-3′
TNF-α	5′-CTCTTCTCATTCCTGCTTGTGG-3′	5′-AATCGGCTGACGGTGTGG-3′
IL6	5′-CGGCCTTCCCTACTTCACAAG-3′	5′-TAACAGATAAGCTGGAGTCACAGAA-3′
Adiponectin	5′-GCCGCTTATGTGTATCGCTCAG-3′	5′-GCCGTGCTGCCGTCATAATG-3′
Leptin	5′ -GGATCAATGACATTTCACACACG-3′	5′-AGGAATGAAGTCCAAGCCAGT-3′

Blood samples were obtained from the tail tip at 0, 15, 30, 60, and 120 minutes for the measurement of blood glucose by using One Touch Ultra glucometer (Lifescan, Inc, USA).

Determination of CCK, GLP-1, PYY, LPS, and Cytokines

An appropriate amount of dipeptidyl peptidase 4 inhibitor DPP4i (EMD Millipore cat. no. DPP4) was added to blood samples immediately to prevent degradation of blood GLP-1. The active GLP-1 content in culture medium and plasma was quantified by enzyme-linked immunosorbent assay (EMD Millipore, cat. no. EGLP-35K, USA). To increase the sensitivity of enzyme-linked immunosorbent assay, 10 pmol/L of GLP-1 standard was added into each cell before doing any assay according to the manufacturer's recommendations (Millipore, France). The PYY (ref. EIAM-PYY-1) and CCK (ref. EIAM-CCK-1) in plasma were determined by enzyme-linked immunosorbent assay as per instructions of the manufacturer (Raybiotech, USA). Plasma LPS was separated by reverse-phase high-performance liquid chromatography and quantitated by liquid chromatography/-mass spectrometry. Briefly, free fatty acids were extracted with 600 μL of distilled water and 5 mL of hexane. Fatty acid separation was performed in an Infinity 1200 HPLC binary system (Agilent) equipped with a Poroshell 120 EC C18 100×4.6 mm 2.7 μm column (Agilent) set at 30°C. The further quantification of LPS involved mass spectrometer. The enzyme-linked immunosorbent assay kits for TNF-α (ref. LS-F12798-1) and IL6 (ref. OKBB00190) were purchased from Clinisciences, France for the determination of their circulating concentrations.

Biochemical Analysis

Urea, creatinine, cholesterol, triglyceride, high-density lipoprotein, low-density lipoprotein, very low-density lipoprotein, aspartate aminotransferase, alanine aminotransferase, alkaline phosphate, and other blood parameters were determined by the University Hospital laboratory by an automated analyzer.

Western Blot Analysis

After death, the TBC were isolated as described before. The cell lysates were prepared in the following buffer: 20 mmol/L HEPES pH 7.3, 1 mmol/L EDTA, 1 mmol/L EGTA, 0.15 mmol/L NaCl, 1% Triton X-100, 10% glycerol, 1 mmol/L phenylmethylsulfonyl fluoride, 2 mmol/L sodium orthovanadate, and 2 mL anti-protease cocktail) and centrifuged (13,000g × 10 minutes). Denatured proteins (30 mg) were separated by sodium dodecyl sulfate-polyacrylamide gel electrophoresis (10%), transferred to polyvinylidene difluoride membranes, and identified with primary anti-CD36 (1:500 dilution) and anti-GPR120 (1:500 dilution) antibodies. Immunoblots were then incubated with a specific horseradish peroxidase–conjugated secondary antibody and developed by using electrochemoluminescent method and reagents according to manufacturer's protocol (PerkinElmer, Waltham, MA).

Histologic Studies

After death, liver and epididymal adipose tissues were collected, fixed in 10% (v/v) neutral-buffered formalin, and embedded in paraffin, and 5- to 6-μm-thick sections were stained by hematoxylin–eosin–safran dyes. The Oil-Red was used to observe lipid accumulation in liver sections. The slides were studied under a light microscope, and the captured images were used for further analyses.

Indirect Calorimetry

Indirect calorimetry was performed using a computer-controlled, open-circuit system (Columbus Oxymax Comprehensive Lab Animal Monitoring System). Mice were individually tested during 24 hours at 23°C ± 0.5°C after being acclimated to the measurement cage over 5 days. Outdoor air reference values were sampled every 8 measurements. Gas sensors were calibrated before experiment with gas standards containing known concentrations of O_2, CO_2, and N_2 (Air Liquide – Certified accuracy ±1%). Data from 5 separate experimental runs were combined. Oxygen consumption (VO_2), carbon dioxide production (VCO_2), total and locomotor activity, and food intake were recorded in time intervals of 20 minutes during the whole measurement period. Energy expenditure

(EE) was calculated as EE = (3.815 + 1.232 × RER) × VO_2. Respiratory exchange ratio (RER) was calculated as the ratio of VCO_2 to VO_2. Energy balance was calculated as EB = food consumed (kcal/h) – EE (kcal/h). Raw data files from Oxymax software were analyzed with CalR (https://calrapp.org).

Analysis of Lean and Fat Mass by EchoMRI

Body lean and fat mass were analyzed by EchoMRI 500 (EchoMRI, Houston, TX). Scans were taken by placing animals in a thin-walled plastic cylinder (3 thick, 6.8 cm inner diameter), with a cylindrical plastic insert added to limit the movement of the animals. Within the tube, the animals were briefly subjected to a low-intensity (0.05 T) electromagnetic field to measure fat mass, lean mass, free water, and total body water as described elsewhere.[15]

Statistical Analyses

Data are presented as mean ± standard error of the mean (SEM). Sample size is indicated in figure legends. Statistical analyses were performed by SPSS software. Unpaired two-tailed Student t test was used to compare 2 experimental groups. One-way or two-way analysis of variance, followed by Tukey multiple comparison test, was applied to compare 3 or more groups. Statistical significance was defined as $P \leq .05$. For indirect calorimetry, the statistical analysis was performed with CalR, a custom package for analysis of indirect calorimetry using analysis of covariance with body weight as covariate to analyze mass-dependent metabolic variables.[61]

All authors had access to the study data and had reviewed and approved the final manuscript.

References

1. Laugerette F, Passilly-Degrace P, Patris B, Niot I, Febbraio M, Montmayeur JP, Besnard P. CD36 involvement in orosensory detection of dietary lipids, spontaneous fat preference, and digestive secretions. J Clin Invest 2005;115:3177–3184.
2. Dramane G, Abdoul-Azize S, Hichami A, Vögtle T, Akpona S, Chouabe C, Sadou H, Nieswandt B, Besnard P, Khan NA. STIM1 regulates calcium signaling in taste bud cells and preference for fat in mice. J Clin Invest 2012;122:2267–2282.
3. Ozdener MH, Subramaniam S, Sundaresan S, Sery O, Hashimoto T, Asakawa Y, Besnard P, Abumrad NA, Khan NA. CD36- and GPR120-mediated $Ca2^+$ signaling in human taste bud cells mediates differential responses to fatty acids and is altered in obese mice. Gastroenterology 2014;146:995–1005.
4. Khan AS, Keast R, Khan NA. Preference for dietary fat: from detection to disease. Prog Lipid Res 2020;78:101032.
5. Besnard P, Passilly-Degrace P, Khan NA. Taste of fat: a sixth taste modality? Physiol Rev 2016;96:151–176.
6. El-Yassimi A, Hichami A, Besnard P, Khan NA. Linoleic acid induces calcium signaling, Src kinase phosphorylation, and neurotransmitter release in mouse CD36-positive gustatory cells. J Biol Chem 2008;283:12949–12959.
7. Gilbertson TA, Khan NA. Cell signaling mechanisms of oro-gustatory detection of dietary fat: advances and challenges. Prog Lipid Res 2014;53:82–92.
8. Khan NA, Besnard P. Oro-sensory perception of dietary lipids: new insights into the fat taste transduction. Biochim Biophys Acta 2009;1791:149–155.
9. Chen CS, Bench EM, Allerton TD, Schreiber AL, Arceneaux KP 3rd, Primeaux SD. Preference for linoleic acid in obesity-prone and obesity-resistant rats is attenuated by the reduction of CD36 on the tongue. Am J Physiol Regul Integr Comp Physiol 2013;305:R1346–R1355.
10. Cartoni C, Yasumatsu K, Ohkuri T, Shigemura N, Yoshida R, Godinot N, le Coutre J, Ninomiya Y, Damak S. Taste preference for fatty acids is mediated by GPR40 and GPR120. J Neurosci 2010;30:8376–8382.
11. Sclafani A, Zukerman S, Ackroff K. GPR40 and GPR120 fatty acid sensors are critical for postoral but not oral mediation of fat preferences in the mouse. Am J Physiol Regul Integr Comp Physiol 2013;305:R1490–R1497.
12. Sclafani A, Ackroff K, Abumrad NA. CD36 gene deletion reduces fat preference and intake but not post-oral fat conditioning in mice. Am J Physiol Regul Integr Comp Physiol 2007;293:R1823–R1832.
13. Stewart JE, Feinle-Bisset C, Keast RS. Fatty acid detection during food consumption and digestion: associations with ingestive behavior and obesity. Prog Lipid Res 2011;50:225–233.
14. Sayed A, Śerý O, Plesnik J, Daoudi H, Rouabah A, Rouabah L, Khan NA. CD36 AA genotype is associated with decreased lipid taste perception in young obese, but not lean, children. Int J Obes (Lond) 2015;39:920–924.
15. Mrizak I, Śerý O, Plesnik J, Arfa A, Fekih M, Bouslema A, Zaouali M, Tabka Z, Khan NA. The A allele of cluster of differentiation 36 (CD36) SNP 1761667 associates with decreased lipid taste perception in obese Tunisian women. Br J Nutr 2015;113:1330–1337.
16. Karmous I, Plesník J, Khan AS, Śerý O, Abid A, Mankai A, Aouidet A, Khan NA. Orosensory detection of bitter in fat-taster healthy and obese participants: genetic polymorphism of CD36 and TAS2R38. Clin Nutr 2018;37:313–320.
17. Bajit H, Ait Si Mohammed O, Guennoun Y, Benaich S, Bouaiti E, Belghiti H, Mrabet M, Elfahime EM, El Haloui NE, Saeid N, El Kari K, Hichami A, Khan NA, Benkirane H, Aguenaou H. Single-nucleotide polymorphism rs1761667 in the *CD36* gene is associated with orosensory perception of a fatty acid in obese and normal-weight Moroccan subjects. J Nutr Sci 2020;9:e24.
18. Plesník J, Śerý O, Khan AS, Bielik P, Khan NA. The rs1527483, but not rs3212018, CD36 polymorphism associates with linoleic acid detection and obesity in Czech young adults. Br J Nutr 2018;119:472–478.
19. Colla K, Costanzo A, Gamlath S. Fat replacers in baked food products. Foods 2018;7:192.
20. Micha R, Khatibzadeh S, Shi P, Fahimi S, Lim S, Andrews KG, Engell RE, Powles J, Ezzati M, Mozaffarian D. Global, regional, and national

consumption levels of dietary fats and oils in 1990 and 2010: a systematic analysis including 266 country-specific nutrition surveys. Br Med J 2014;348:g2272.
21. Cunningham AL, Stephens JW, Harris DA. A review on gut microbiota: a central factor in the pathophysiology of obesity. Lipids Health Dis 2021;20:65.
22. Everard A, Belzer C, Geurts L, Ouwerkerk JP, Druart C, Bindels LB, Guiot Y, Derrien M, Muccioli GG, Delzenne NM, de Vos WM, Cani PD. Cross-talk between Akkermansia muciniphila and intestinal epithelium controls diet-induced obesity. Proc Natl Acad Sci U S A 2013;110:9066–9071.
23. Dao MC, Everard A, Aron-Wisnewsky J, Sokolovska N, Prifti E, Verger EO, Kayser BD, Levenez F, Chilloux J, Hoyles L, MICRO-Obes Consortium, Dumas ME, Rizkalla SW, Doré J, Cani PD, Clément K. Akkermansia muciniphila and improved metabolic health during a dietary intervention in obesity: relationship with gut microbiome richness and ecology. Gut 2016;65:426–436.
24. Samra RA. Fats and satiety. In: Montmayeur JP, le Coutre J, eds. Fat detection: taste, texture, and post ingestive effects. Boca Raton, FL: CRC Press/Taylor & Francis, 2010.
25. Godinot N, Yasumatsu K, Barcos ME, Pineau N, Ledda M, Viton F, Ninomiya Y, le Coutre J, Damak S. Activation of tongue-expressed GPR40 and GPR120 by non caloric agonists is not sufficient to drive preference in mice. Neuroscience 2013;250:20–30.
26. Cornall LM, Mathai ML, Hryciw DH, McAinch AJ. GPR120 agonism as a countermeasure against metabolic diseases. Drug Discov Today 2014;19:670–679.
27. Cornall LM, Mathai ML, Hryciw DH, McAinch AJ. Diet-induced obesity up-regulates the abundance of GPR43 and GPR120 in a tissue specific manner. Cell Physiol Biochem 2011;28:949–958.
28. Murtaza B, Hichami A, Khan AS, Shimpukade B, Ulven T, Ozdener MH, Khan NA. Novel GPR120 agonist TUG891 modulates fat taste perception and preference and activates tongue-brain-gut axis in mice. J Lipid Res 2020; 61:133–142.
29. Reed DR, Xia MB. Recent advances in fatty acid perception and genetics. Adv Nutr 2015;6:353S–360S.
30. Berthoud HR, Morrison CD, Ackroff K, Sclafani A. Learning of food preferences: mechanisms and implications for obesity & metabolic diseases. Int J Obes (Lond) 2021;45:2156–2168.
31. Ogawa N, Ito M, Yamaguchi H, Shiuchi T, Okamoto S, Wakitani K, Minokoshi Y, Nakazato M. Intestinal fatty acid infusion modulates food preference as well as calorie intake via the vagal nerve and midbrain-hypothalamic neural pathways in rats. Metabolism 2012;61:1312–1320.
32. Desai AJ, Dong M, Harikumar KG, Miller LJ. Cholecystokinin-induced satiety, a key gut servomechanism that is affected by the membrane microenvironment of this receptor. Int J Obes Suppl 2016;6(Suppl 1):S22–S27.
33. Zander M, Madsbad S, Madsen JL, Holst JJ. Effect of 6-week course of glucagon-like peptide 1 on glycaemic control, insulin sensitivity, and beta-cell function in type 2 diabetes: a parallel-group study. Lancet 2002;359:824–830.
34. Torang S, Bojsen-Møller KN, Svane MS, Hartmann B, Rosenkilde MM, Madsbad S, Holst JJ. In vivo and in vitro degradation of peptide YY3-36 to inactive peptide YY3-34 in humans. Am J Physiol Regul Integr Comp Physiol 2016;310:R866–R874.
35. Régnier M, Van Hul M, Knauf C, Cani PD. Gut microbiome, endocrine control of gut barrier function and metabolic diseases. J Endocrinol 2020; JOE-20-0473.R1.
36. Tappenden KA, McBurney MI. Systemic short-chain fatty acids rapidly alter gastrointestinal structure, function, and expression of early response genes. Dig Dis Sci 1998;43:1526–1536.
37. Derrien M, Belzer C, de Vos WM. Akkermansia muciniphila and its role in regulating host functions. Microb Pathog 2017;106:171–181.
38. Song X, Zhong L, Lyu N, Liu F, Li B, Hao Y, Xue Y, Li J, Feng Y, Ma Y, Hu Y, Zhu B. Insulin can alleviate metabolism disorders in ob/ob mice by partially restoring leptin-related pathways mediated by gut microbiota. Genomics, Proteomics & Bioinformatics 2019;17:64–75.
39. Shen F, Zheng RD, Sun XQ, Ding WJ, Wang XY, Fan JG. Gut microbiota dysbiosis in patients with non-alcoholic fatty liver disease. Hepatob Pancreatic Dis Int 2017;16:375–381.
40. Ortega-Hernández A, Martínez-Martínez E, Gómez-Gordo R, López-Andrés N, Fernández-Celis A, Gutiérrez-Miranda B, Nieto ML, Alarcón T, Alba C, Gómez-Garre D, Cachofeiro V. The interaction between mitochondrial oxidative stress and gut microbiota in the cardiometabolic consequences in diet-induced obese rats. Antioxidants (Basel) 2020;9:640.
41. Vinolo MA, Rodrigues HG, Nachbar RT, Curi R. Regulation of inflammation by short chain fatty acids. Nutrients 2011;3:858–876.
42. Inoue M, Ohtake T, Motomura W, Takahashi N, Hosoki Y, Miyoshi S, Suzuki Y, Saito H, Kohgo Y, Okumura T. Increased expression of PPARgamma in high fat diet-induced liver steatosis in mice. Biochem Biophys Res Commun 2005;336:215–222.
43. Fraulob JC, Ogg-Diamantino R, Fernandes-Santos C, Aguila MB, Mandarim-de-Lacerda CA. A mouse model of metabolic syndrome: insulin resistance, fatty liver and non-alcoholic fatty pancreas disease (NAFPD) in C57BL/6 mice fed a high fat diet. J Clin Biochem Nutr 2010;46:212–223.
44. Park EJ, Lee JH, Yu GY, He G, Ali SR, Holzer RG, Osterreicher CH, Takahashi H, Karin M. Dietary and genetic obesity promote liver inflammation and tumorigenesis by enhancing IL-6 and TNF expression. Cell 2010; 140:197–208.
45. Sadek MA, Darwish SF, Abd El-Rhman A, Ismail Abo El-Fadl HM. Impact of different dietary components on gene expression of leptin and adiponectin in adipose tissue of obese rats. Int J Biochem Res Rev 2016;15:1–15.
46. Zhang C, Mortuza SM, He B, Wang Y, Zhang Y. Template-based and free modeling of I-TASSER and QUARK pipelines using predicted contact maps in CASP12. Proteins 2018;86(Suppl 1):136–151.
47. Ko J, Park H, Heo L, Seok C. GalaxyWEB server for protein structure prediction and refinement. Nucleic Acids Res 2012;40(Web Server issue):W294–W297.

48. Polyansky AA, Volynsky PE, Efremov RG. Multistate organization of transmembrane helical protein dimers governed by the host membrane. J Am Chem Soc 2012;134:14390–14400.
49. Lee J, Cheng X, Swails JM, Yeom MS, Eastman PK, Lemkul JA, Wei S, Buckner J, Jeong JC, Qi Y, Jo S, Pande VS, Case DA, Brooks CL 3rd, MacKerell AD Jr, Klauda JB, Im W. CHARMM-GUI input generator for NAMD, GROMACS, AMBER, OpenMM, and CHARMM/OpenMM simulations using the CHARMM36 additive force field. J Chem Theory Comput 2016;12:405–413.
50. Doobay M, Cross-Mellor SK, Wah DTO, Kavaliers M, Ossenkopp KP. Toxin-induced aversive context conditioning: assessing active aversive behaviors conditioned to the context of an automated activity –monitor. Physiol Behav 2021;240:113559.
51. Tao N, Wagner SJ, Lublin DM. CD36 is palmitoylated on both N- and C-terminal cytoplasmic tails. J Biol Chem 1996;271:22315–22320.
52. Yesylevskyy SO. Pteros 2.0: evolution of the fast parallel molecular analysis library for C++ and python. J Comput Chem 2015;36:1480–1488.
53. Valentin-Severin I, Le Hegarat L, Lhuguenot JC, Le Bon AM, Chagnon MC. Use of HepG2 cell line for direct or indirect mutagens screening: comparative investigation between comet and micronucleus assays. Mutat Res 2003;536:79–90.
54. Kirsch-Volders M, Sofuni T, Aardema M, Albertini S, Eastmond D, Fenech M, Ishidate M Jr, Lorge E, Norppa H, Surrallés J, von der Hude W, Wakata A. Report from the In Vitro Micronucleus Assay Working Group. Environ Mol Mutagen 2000;35:167–172.
55. Ames BN, Mccann J, Yamasaki E. Methods for detecting carcinogens and mutagens with the Salmonella/mammalian-microsome mutagenicity test. Mutat Res 1975;31:347–364.
56. Ancel D, Bernard A, Subramaniam S, Hirasawa A, Tsujimoto G, Hashimoto T, Passilly-Degrace P, Khan NA, Besnard P. The oral lipid sensor GPR120 is not indispensable for the orosensory detection of dietary lipids in mice. J Lipid Res 2015;56:369–378.
57. Ullah H, Khan AS, Murtaza B, Hichami A, Khan NA. Tongue leptin decreases oro-sensory perception of dietary fatty acids. Nutrients 2021;14:197.
58. Hichami A, Murtaza B, Khan AS, Zwetyenga N, Khan NA. Development of a human fungiform taste bud cell line: characterization and cell physiological studies. Presented at the Europhysiology, London. IP is protected by INPI (France) no. DSO2021002050 dated 04/02/2021. Cells submitted to the national bank at Institut Pasteur (Paris) CNCM no. I-5485, dated 05/02/2020. Regional Human Ethical Committee (Grand-Est), protocol approval no. RCB2017-A00458-45 2018:14–16.
59. Kusuhara Y, Yoshida R, Ohkuri T, Yasumatsu K, Voigt A, Hübner S, Maeda K, Boehm U, Meyerhof W, Ninomiya Y. Taste responses in mice lacking taste receptor subunit T1R1. J Physiol 2013;591:1967–1985.
60. Subramaniam S, Ozdener MH, Abdoul-Azize S, Saito K, Malik B, Maquart G, Hashimoto T, Marambaud P, Aribi M, Tordoff MG, Besnard P, Khan NA. ERK1/2 activation in human taste bud cells regulates fatty acid signaling and gustatory perception of fat in mice and humans. FASEB J 2016;30:3489–3500.
61. Mina AI, LeClair RA, LeClair KB, Cohen DE, Lantier L, Banks AS. CalR: A Web-based analysis tool for indirect calorimetry experiments. Cell Metab 2018;28:656–666.e1.

Received June 21, 2022. Accepted November 10, 2022.

Correspondence
Address correspondence to: Naim Khan, PhD, DSc, U1231 INSERM, Physiologie de la Nutrition & Toxicologie (NUTox), Université de Bourgogne-Franche Comté (UBFC), Dijon 21000, France. e-mail: Naim.Khan@u-bourgogne.fr.

Acknowledgements
The authors thank Miss Charmaine Bastian Joseph, Miss Anoucheka Bories, Baptiste Rugeri, and Mr Anthony-Damien Desirée for their technical assistance.
Present affiliation for Julia Leemput: Team PADYS, UMR UB/AgroSup/INSERM U1231, Lipides, Nutrition & Cancer, Université de Bourgogne-Franche Comté (UBFC), Dijon, France.

CRediT Authorship Contributions
Naim Khan, PhD, DSc (Conceptualization: Lead; Formal analysis: Lead; Investigation: Equal; Project administration: Lead; Supervision: Lead; Writing – original draft: Lead)
Amira Sayed Khan, PhD (Formal analysis: Equal; Methodology: Equal; Validation: Lead)
Aziz Hichami, PhD (Conceptualization: Equal; Data curation: Lead; Formal analysis: Equal; Validation: Lead)
Babar Murtaza, PhD (Investigation: Equal; Methodology: Equal)
Marie-Laure Louillat-Habermeyer, PhD (Investigation: Lead; Validation: Lead)
Christophe Ramseyer, PhD (Data curation: Equal; Investigation: Lead; Methodology: Equal)
Maryam Azadi, PhD (Investigation: Lead; Methodology: Equal; Validation: Lead)
Semen Yesylevskyy, PhD (Data curation: Equal; Investigation: Lead; Validation: Equal)
Floriane Mangin, PhD (Conceptualization: Equal; Investigation: Equal; Methodology: Equal)
Frederic Lirussi, PhD (Data curation: Equal; Software: Lead; Validation: Lead)
Julia Leemput, PhD (Data curation: Supporting; Methodology: Supporting)
Jean-Francois Merlin, PhD (Data curation: Equal; Formal analysis: Equal)
Antonin Schmitt, PhD (Formal analysis: Supporting; Methodology: Supporting)
Muhtadi Suliman, PhD (Investigation: Equal; Methodology: Equal)
Jérôme Bayardon, PhD (Formal analysis: Equal; Validation: Supporting)
Saeed Semnanian, PhD (Investigation: Equal; Methodology: Equal; Supervision: Equal)
Sylvain Jugé, PhD (Conceptualization: Equal; Data curation: Equal; Investigation: Equal; Supervision: Equal; Writing – original draft: Equal)

Conflicts of interest
The authors disclose no conflicts.

Funding
Supported by financial support from the SATT (Société d'Accélération du Transfert de Technologies) Grand-Est (Dijon) that financed two projects (ImmorTasteCell and FaTasteAnalogues). This project was also supported by the University of Burgundy as BQR (bonus-qualité-recherche). The DRRT (délégation régionale à la recherche et à la technologie) at Dijon granted a project on the synthesis of fat taste agonists. The BFC (Burgundy Franche Comté) Région also granted a post-doc scholarship to one of the authors (MS). The BFC (Burgundy Franche Comté) Région also sanctioned a project "Tasty Lipids" in the category "Envergeure" that helped realize research work. A grant for the recruitment of a technician is also acknowledged from LipStick Excellence laboratory (ANR-11-LABX-0021-LipSTIC). SY was supported by the European Union's Horizon 2020 research and innovation program under the Marie Skłodowska-Curie grant agreement no. 796245 and the NATO SPS grant no. 985291. The computations were performed using HPC resources from the Centre de Calcul Régional Romeo and the Mésocentre de Calcul de Franche-Comté.